Bulletin of Engineering Geology and the Environment (2021) 80:4651–4672
https://doi.org/10.1007/s10064-021-02230-5

ORIGINAL PAPER

A simplified analytical solution for deformation behavior of existing tunnels subjected to influences of landslides

Zhiguo Zhang[1,2,3,4] · Mengxi Zhang[5] · Qihua Zhao[3] · Lei Fang[1] · Shaokun Ma[6] · Xilin Lv[7]

Received: 8 September 2020 / Accepted: 28 March 2021 / Published online: 17 April 2021

Abstract

Current scholars have made more efforts to investigate the deformation of landslide caused by tunnel excavation, but there are few studies on the mechanical properties of existing tunnels subjected to influences of landslides. Furthermore, very little attention is paid to the simplified analytical solution for landslide-tunnel interaction and current studies still remain on the monitoring and numerical modeling of engineering. A simplified analytical method is proposed in this paper to evaluate on the deformation of existing tunnels induced by landslides. Firstly, the landslide thrust sliding forces are calculated based on the transferring coefficient method and the limit equilibrium method. Secondly, imposing the thrust sliding force on the existing tunnels, the elastic foundation beam model is established for predicting the landslide-tunnel interaction. Then, the internal force and displacement for the existing tunnels caused by the landslides are solved by the transfer matrix method. In addition, the three-dimensional numerical simulation results are compared with the simplified analytical solution and good consistency is obtained. Furthermore, the parametric analysis for influences of the cohesive force, the internal friction angle, and the unit weight of landslide body is conducted on the thrust sliding force. The influences of the thrust sliding force, the foundation coefficient of landslide and sliding bed, the tunnel lining stiffness, and the tunnel length on the existing tunnels are also analyzed with the parametric analyses by the simplified analytical solution. The paper contributes to the understanding of interaction mechanics for landslides as a potential risk in preliminary design of tunnels.

Keywords Existing tunnel · Mountainous landslide · Tunnel-landslide interaction · Transfer matrix method · Simplified analytical solution

✉ Zhiguo Zhang
zgzhang@usst.edu.cn

[1] School of Environment and Architecture, University of Shanghai for Science and Technology, 516 Jungong Road, Shanghai 200093, China

[2] Department of Civil and Environmental Engineering, National University of Singapore, Singapore, Singapore

[3] State Key Laboratory of Geohazard Prevention and Geoenvironment Protection, Chengdu University of Technology, Chengdu 610059, Sichuan, China

[4] Key Laboratory of Geohazard Prevention of Hilly Mountains, Ministry of Natural Resources, Fujian Key Laboratory of Geohazard Prevention, Fuzhou 350002, China

[5] School of Mechanics and Engineering Science, Shanghai University, Shanghai 200444, China

[6] School of Civil Engineering and Architecture, Guangxi University, Nanning 530004, Guangxi, China

[7] Department of Geotechnical Engineering, Tongji University, Shanghai 200092, China

Introduction

With the sharp demanding of worldwide transportation, more and more railways and highways have to cross mountainous areas. Then, it is common to encounter the special geological cases for the mountain slopes and landslides. In general, tunnels should be avoided to construct in the landslide zone. However, some tunnels inevitably need to cross the landslide zone during construction. In addition, under the influences of geological evolution and excavation disturbance loads, the existing slopes with no obvious displacement or relatively stable condition will have large deformation and even develop into landslides. Then, it may cause different degrees of damage for the existing tunnel structures, affecting and even interrupting the normal operation of the tunnels. Therefore, it is vital to put forward a method for estimating the deformation of existing tunnels induced by landslides in mountain region.

The excavation of a tunnel and deep excavation causes the stress redistribution, inducing deformation in the ground surrounding the opening and additional influences on the adjacent structures (Fang et al. 2016; Song et al. 2018; Lu et al. 2019; Wu et al. 2019; Jin et al. 2020). In areas prone to instability, the induced stress state can trigger or accelerate landslide movements, even on a large scale (Bandini et al. 2015). In the research on the landslide or surface deformation induced by the tunnel excavation, the methods may be classified into four categories: on-site measurement, numerical simulation, experience formula, and theoretical analysis. Some attempts have been made to develop the researches about the on-site measurements (Bandini et al. 2015; Bayer et al. 2017; Barla 2018; Lai et al. 2018; Li et al. 2019). On-site measurement methods are mostly based on field observations and intuitive deductions and they are lacking in theory and ambiguous in range of applicability. In addition, the complexity of soil behavior has encouraged the widespread use of numerical modeling analyses, particularly FEM and FLAC. Therefore, the existing results are more focused on numerical simulation methods (Gonzalez and Sagaseta 2001; Ng et al. 2004; Yoo and Kim 2008; Dang and Meguid 2008; Koizumi et al. 2010; Gui and Chen 2013; Do et al. 2014; Causse et al. 2015; Hajjar et al. 2015; Shahin et al. 2016; Zhang et al. 2017; Barla 2018). Although powerful numerical methods undoubtedly provide the most comprehensive simulation for tunnel excavation processes, their predictive accuracy is also closely tied to the knowledge of in situ conditions and the modeling of soil behavior. The theoretical analysis method is an effective practical approach to analyze the tunneling-induced ground deformation through a clear theoretical derivation. Some scholars adopted some empirical formulas to predict the influence of tunnel excavation on surface settlement (Peck 1969; Yoshikoshi et al. 1978; Mair et al. 1993; Vorster et al. 2005; Lai et al. 2017). Four main categories exist for the analytical methods: the virtual image technique (Sagaseta 1987; Verruijt and Booker 1996; Loganathan and Poulos 1998), the complex variable method (Verruijt 1997, 1998; Strack and Verruijt 2002; Wang et al. 2009; Wang and Li 2009; Fu et al. 2015; Zhang et al. 2018), the stress function method using polar coordinates (Bobet 2001; Chou and Bobet 2002; Park 2004, 2005), and the stochastic medium theory (Yang et al. 2004; Yang and Wang 2011).

Landslides can cause considerable damage to buildings and infrastructure. Therefore, many scholars began to study the impacts of landslides on the surrounding obstacles and existing tunnels. Puzrin and Schmid (2012) proposed if the obstacle is rigid and the long-term safety factor of the landslide is lower than one, the earth pressure eventually equals the passive pressure. The problem of the limiting landslide pressure on an obstacle has also been tackled through theoretical (Friedli et al. 2017) and numerical (Muraro et al. 2015) analyses in simplified 2D conditions and for a cohesionless landslide. Galli and Di (2013) analyzed the relationship between landslide displacements and the reaction force from the retaining structure by introducing a characteristic function. In recent years, relevant scholars have begun to pay attention to the influence of tunnel structure deformation in landslide areas. The effects of landslides on civil infrastructure, including tunnels, have been summarized by many researchers (e.g., landslide-pipeline interaction in O'Rourke and Lane 1989 and Casamichele et al. 2004; case histories of landslide-building interaction in Antronico et al. 2015; general aspects of the interaction of landslides and man-made works in Urciuoli and Picarelli 2008; general aspects of landslide-tunnel interaction in Picarelli et al. 2002 and Mouratidis 2008; and case histories of landslide-tunnel interaction in Wang et al. 2001; and Poisel et al. 2016). In the field measurement research, Noferini et al. (2007) used ground SAR (GB-SAR) interferometer to measure the surface displacements of a landslide occurring in the Carnian Alps, north-eastern Italy, and the impact of landslides on tunnels under excavation was monitored. Wang (2010) enumerated the actual engineering of four tunnel axes and different spatial positions of the slope sliding displacement, and studied the characteristics of tunnel lining cracks under the influence of landslide and the effect of crack repair and reinforcement. Chiu et al. (2017) used the on-site monitoring of the No. 20 expressway tunnel in Taiwan as an example to analyze the crack development and spalling of the tunnel lining under the influence of landslide, and proposed landslide-tunnel reinforcement measures. In the research of theoretical methods in the above fields, Vassallo et al. (2016) used finite element numerical simulation method and simplified theoretical method to study the safety impact of landslide motion on railway tunnels. Kong et al. (2018) proposes a displacement function, which is expressed by Fourier series, to describe the cross-section deformation mode of circular shallow buried tunnel with slope surface. Feng et al. (2019) proposed a numerical method to simulate the runout process of flow slide, and the interactions between flow slide and buildings on three-dimensional terrain considering the destruction process. While the effects of landslide on existing tunnel are frequently described in the literature, the studies on the mechanical properties of existing tunnel structures under the action of landslide bodies are rare to conduct in detail, especially the mechanism research of related theoretical analysis. In fact, most of the impacts of the landslide on the existing tunnels remain in the field of actual engineering monitoring. It has been seldom seen to use the theoretical analytical method to analyze the tunnel-landslide interaction.

The landslide-tunneling interaction is a rather complex issue, since it may be influenced by not only the geological condition and the construction environment, but also the tunnel structure design and the tunnel excavation process. Current investigation has paid more attention to the deformation of landslide bodies induced by tunnel excavation, but

there are few studies on the mechanical properties of existing tunnels due to the landslides. Furthermore, little investigation are given to detailed theoretical analysis of landslide-tunnel interactions from geotechnical and structural perspectives and most studies focus on the monitoring and numerical solution for practical engineering. Zhang et al. (2017) carried out the landslide-tunnel interaction analyses by the analytical and numerical methods to assess the safe distance of a tunnel from the landslide slip surface. The study of Zhang et al. (2017) aims to analyze the geo-environmental of landslides caused by tunneling; however, the deformation of existing tunnels due to sliding forces of landslides is still not considered. In this paper, the interaction between landslide and tunnel is observed in detail by analytical and numerical methods, and a simplified theoretical method is proposed for obtaining the deformation of existing tunnel structures induced by landslides. The tunnel model is simplified into an elastic foundation beam, and the tunnel-slide interaction is simulated by soil spring. Firstly, the transfer coefficient method and the limit equilibrium method are used to calculate the magnitude of the landslide thrust sliding force, and the influence of landslide cohesive force, internal friction angle, and unit weight on landslide thrust sliding force are conducted. Secondly, the landslide thrust sliding force calculated in the previous stage is applied to the tunnel structure, and the tunnel model that has been simplified to the elastic foundation beam is calculated by the transfer matrix method. Furthermore, the numerical simulation analysis is enforced to verify the effectiveness of the simplified analytical method and the influencing factors of some key parameters are analyzed by the simplified solution.

Thrust sliding force due to landslide

In this study for the deformation behavior of existing tunnels induced by landslides, the landslide thrust sliding force is firstly analyzed. At present, the calculation method of the landslide thrust sliding force mainly includes the transfer coefficient method (Song and Xu 2012; Wang et al. 2016), the limit equilibrium method, and the finite element method. The transfer coefficient method is widely used because of its clear concept and convenient calculation, especially for the folded-line landslide. Since the modeling in this study is assumed as folded-line landslide, the transfer coefficient method is used for analysis of the landslide thrust sliding force. The limit equilibrium method is used for analysis of the single slide mass element.

The main hypothesis is listed as below: (1) The landslide is divided into several vertical slices along the sliding direction of the landslide. The force of each slice is analyzed and the equilibrium equation is obtained. The residual resultant force along the sliding direction on the interface is calculated as the landslide thrust sliding force of the slide mass. (2) Since it can be approximately simplified to a plane strain problem, the transverse length of the vertical slide mass is taken for per unit width. The forces acting on the lateral adjacent landslides are not considered in this study. (3) It is assumed that the landslide thrust sliding force on the interface of all vertical slide mass is rectangular distribution, and the direction of the residual landslide thrust sliding force of the bars is parallel to the inclined direction of the sliding surface.

Calculation theory of landslide thrust sliding force

According to the above assumptions, a vertical slide mass is taken for the force analysis, as shown in Fig. 1. The parameter q'_i (kN/m) is the reaction force between the i-th slide mass and the i-1th slide mass, the direction points to sliding upward and parallels to the i-th slide mass sliding surface. The parameter q_i (kN/m) is defined as the landslide thrust sliding force per meter of the i-th slide mass, which is equal to q'_i in the opposite direction. For $q_i \le 0$, no sliding occurs under a given safety coefficient; for $q_i > 0$, sliding will occur under given safety coefficient. The parameter $q_{i\text{-}1}$ (kN/m) is the residual sliding force per meter of the i-1th slide mass, the direction points to

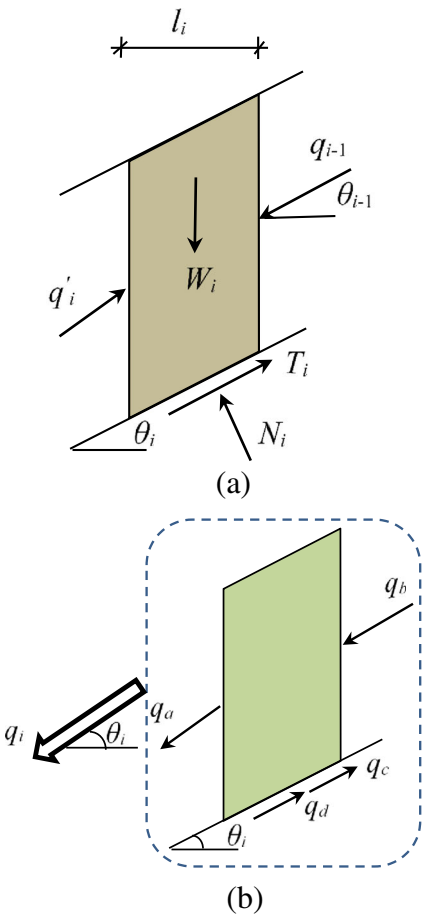

Fig. 1 Force analysis of a slide mass. **a** Analysis of the whole force for i unit. **b** Composition of landslide thrust sliding force per meter for i unit

sliding downward and parallels to the i-1th slide mass sliding surface. The parameter θ_i is the inclination angle of the sliding surface of the i-th slide mass, and θ_{i-1} is the inclination angle of the sliding surface of the i-1th slide mass. The landslide thrust sliding force (Fig. 1b) can be expressed as:

$$q_i = q_a + q_b + q_c + q_d \quad (1)$$

$$q_a = KW_i \sin(\theta_i) \quad (2)$$

$$q_b = q_{i-1}[cos(\theta_{i-1}-\theta_i) - sin(\theta_{i-1}-\theta_i)tan\varphi_i] \quad (3)$$

$$q_c = -W_i \cos\theta_i \tan\varphi_i \quad (4)$$

$$q_d = -c_i l_i \quad (5)$$

$$\psi_i = cos(\theta_{i-1}-\theta_i) - sin(\theta_{i-1}-\theta_i)tan\varphi_i \quad (6)$$

where q_a (kN/m) is the sliding force per meter produced by the i-th slide mass; q_b (kN/m) is the sliding force or the upward sliding force per meter produced by the i-1th slide mass; q_c (kN/m) is the anti-sliding force per meter of the i-th slide mass; q_d (kN/m) is the anti-sliding force per meter produced by the sliding surface of the i-th slide mass. The q_c and q_d are derived from the Mohr-Coulomb criterion. The angle of q_a, q_b, q_c, q_d with the horizontal plane is θ_i. K is the safety coefficient needed in calculation of anti-sliding force; W_i (kN/m) is the per-meter weight of the i-th slide mass; φ_i is the friction angle on the sliding surface of the i-th slide mass; c_i (kPa) is the cohesive force on the sliding surface of the i-th slide mass; l_i (m) is the length of the sliding surface where the i-th slide mass is located; ψ_i is the transfer coefficient for residual sliding force.

Case analyses

Based on the above method, the following landslide model analyses are established, as shown in Fig. 2. According to the geometric shape and failure form of landslide, it is divided into 20 elements for calculation. The slope line is divided into three sections, and their lengths are defined as s_1, s_2, and s_3. The sliding surface is divided into three sections, and their lengths are defined as s_4, s_5, and s_6. The basic calculation parameters are as follows: the landslide weight is 20 kN/m^3; s_1 = 14.94 m, s_2 = 9.35 m, s_3 = 12.17 m; s_4 = 9.06 m, s_5 = 10.37 m, s_6 = 13.62 m; the internal friction angle of the sliding surface φ = 20°; the cohesive force at the sliding surface c = 100 kPa. The specific parameters are shown in Table 1.

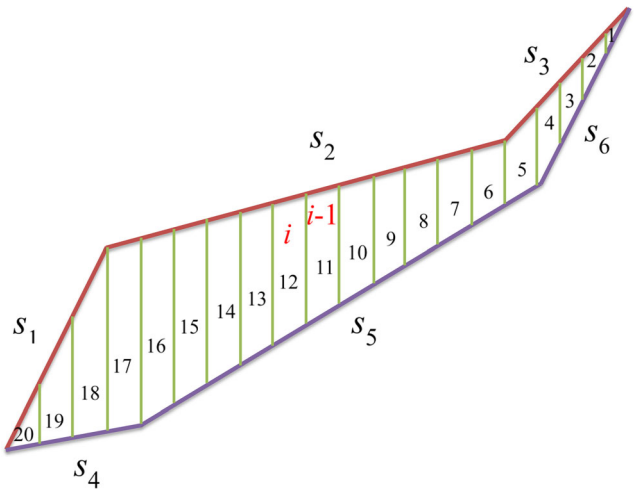

Fig. 2 Landslide geometry and segmentation

According to Fig. 2, the residual landslide thrust of each vertical slide mass can be calculated by dividing the landslide and combining Eqs. (1)–(6). The calculation results under different safety coefficients are shown in Tables 2, 3, and 4. The parameter q_a (kN/m) is the sliding force per meter produced by the i-th slide mass; q_b (kN/m) is the sliding force or the upward sliding force per meter of the i-1th slide mass; q_c (kN/m) is the anti-sliding force per meter of the i-th slide mass; q_d (kN/m) is the anti-sliding force per meter produced by the sliding surface of the i-th slide mass.

The relationship curves between the landslide thrust and the safety coefficient are drawn based on Tables 1, 2, 3, and 4, as shown in Fig. 3. The figure shows that the greater the safety coefficient is, the greater the landslide thrust will be, and the greater the landslide unstable area will be. When K is set as 1.0, the unstable region of the landslide is basically falling between the number i = 10~17; when K is set as 1.1, the unstable region expands to the region numbered i = 8~18; when K is set as 1.2, the range of unstable region is numbered i = 6~20. The position where the landslide thrust change is obvious at the 16th slide mass, where the slope of the sliding surface turns, and it has a great impact on the landslide thrust sliding force. We can find that the larger the safety coefficient is, the smaller the deformation allowed for the landslide is, and the larger the unstable area of the landslide is. It is shown in Eq. (2) that the safety reserve is actually directly attached to the sliding force generated by gravity in the calculation process.

Influencing factor analyses of landslide thrust sliding force

The basic parameters are setting: the internal friction angle φ is 20°, the cohesive force c is 100 kPa, and the unit weight γ is 20 kN/m^3. One of the three parameters is changed separately, and the other parameters are unchanged to observe the influences of different parameters on the landslide thrust sliding force.

(1) Influence of cohesive force on landslide thrust sliding force

It can be seen from Fig. 4 that the cohesive force has a great influence on the value and distribution of the landslide thrust sliding force. The landslide thrust sliding force gradually

Table 1 Slide mass geometry parameters

Number	Inclination (°)	Area (mm^2)	Sliding surface length (m)	Weight per meter (kN/m)
1	62.88	15.95	13.62	318.992
2	62.88	47.85	13.62	956.974
3	62.88	79.75	13.62	1594.958
4	62.88	111.65	13.62	2232.94
5	31.4	162.55	10.37	3250.964
6	31.4	164.86	10.37	3297.266
7	31.4	191.06	10.37	3821.21
8	31.4	217.26	10.37	4345.154
9	31.4	243.45	10.37	4869.098
10	31.4	269.65	10.37	5393.042
11	31.4	295.85	10.37	5916.986
12	31.4	322.05	10.37	6440.93
13	31.4	348.24	10.37	6964.874
14	31.4	374.44	10.37	7488.818
15	31.4	400.64	10.37	8012.762
16	31.4	426.84	10.37	8536.706
17	10.62	438.83	9.06	8776.55
18	10.62	369.94	9.06	7398.758
19	10.62	222.13	9.06	4442.656
20	10.62	74.04	9.06	1480.886

decreases with the increase of the cohesive force. This is mainly because the change of the cohesive force can affect the anti-sliding force. The greater the cohesive force, the greater the anti-sliding force, then the larger the blocking effects on the landslide. From the distribution of landslide thrust sliding force, it can be seen that when c is 100 kPa, the distribution range of landslide thrust sliding force is numbered i = 10~17; when c is 70 kPa, the distribution range of landslide thrust sliding force is numbered i = 3~18; when c is 50kPa, the distribution range of landslide thrust sliding force is numbered i = 2~20.

(2) Influence of internal friction angle on landslide thrust sliding force

It is shown in Fig. 5 that the internal friction angle has a great influence on the landslide thrust sliding force. The internal friction angle of the sliding surface mainly affects the anti-sliding force. When the internal friction angle is larger, the anti-sliding resistance is larger, and the landslide is relatively stable. As shown in Fig. 5, as the internal friction angle increases, the landslide thrust gradually decreases, and the distribution range of the landslide thrust also changes. When φ is 20° and φ is 15°, the distribution range of landslide thrust sliding force is mainly between i = 4 and i = 20; when φ is 10°, the distribution range of landslide thrust sliding force is mainly between i = 10 and i = 17.

Table 2 Calculation of landslide thrust sliding force at K = 1.0

Number	Residual sliding force q_i(kN/m)	q_a (kN/m)	q_b (kN/m)	q_c (kN/m)	q_d (kN/m)	Transfer coefficient ψ_i
10	97.39	2809.83	0.00	-1675.44	-1037	1.00
11	304.98	3082.81	97.39	-1838.21	-1037	1.00
12	622.78	3355.79	304.98	-2000.98	-1037	1.00
13	1050.79	3628.77	622.78	-2163.76	-1037	1.00
14	1589.01	3901.75	1050.79	-2326.53	-1037	1.00
15	2237.43	4174.73	1589.01	-2489.30	-1037	1.00
16	2996.07	4447.71	2237.43	-2652.07	-1037	1.00

Table 3 Calculation of landslide thrust sliding force at $K = 1.1$

Number	Residual sliding force q_i(kN/m)	q_a (kN/m)	q_b (kN/m)	q_c (kN/m)	q_d (kN/m)	Transfer coefficient ψ_i
8	103.36	2490.25	0.00	− 1349.90	− 1037	1.00
9	344.22	2790.53	103.36	− 1512.67	− 1037	1.00
10	722.59	3090.81	344.22	− 1675.44	− 1037	1.00
11	1238.46	3391.09	722.59	− 1838.21	− 1037	1.00
12	1891.84	3691.37	1238.46	− 2000.98	− 1037	1.00
13	2682.73	3991.64	1891.84	− 2163.76	− 1037	1.00
14	3611.12	4291.92	2682.73	− 2326.53	− 1037	1.00
15	4677.02	4592.20	3611.12	− 2489.30	− 1037	1.00
16	5880.42	4892.48	4677.02	− 2652.07	− 1037	1.00
17	2472.09	1779.22	4738.56	− 3139.69	− 906	0.81
18	419.20	1499.91	2472.09	− 2646.80	− 906	1.00

(3) Influence of landslide unit weight on landslide thrust sliding force

Figure 6 shows that the greater the landslide unit weight, the greater the landslide thrust sliding force. When γ is 25 kN/m^3, the distribution range of landslide thrust sliding force is mainly between $i = 3$ and $i = 18$; the maximum landslide thrust sliding force is about 6×10^3 kN/m. When γ is 20 kN/m^3, the distribution range of landslide thrust sliding force is mainly between $i = 10$ and $i = 17$; the maximum landslide thrust sliding force is about 3×10^3 kN/m. The unit weight of the landslide mainly affects the value of the sliding force by landslide gravity.

Deformation behavior of existing tunnels induced by landslides

Transfer matrix method for solving elastic foundation beam

The elastic foundation beam model is an important approach to solve the interaction between tunnels and landslides. In this study, the tunnel structure is simplified into a foundation beam, and the tunnel-landslide interaction is simulated by the spring. Considering the sliding direction of landslide is perpendicular to the tunnel axis, the tunnel is in the most unfavorable state of stress and the longitudinal deformation is obvious. Therefore, the axial direction of the tunnel perpendicular to the sliding direction of the landslide is selected in

Table 4 Calculation of landslide thrust sliding force at $K = 1.2$

Number	Residual sliding force q_i(kN/m)	q_a (kN/m)	q_b (kN/m)	q_c (kN/m)	q_d (kN/m)	Transfer coefficient ψ_i
3	76.89	1703.52	0.00	− 264.63	− 1362	1.00
4	729.33	2384.92	76.89	− 370.48	− 1362	1.00
5	468.94	2032.54	483.37	− 1009.97	− 1037	0.66
6	469.07	2061.49	468.94	− 1024.35	− 1037	1.00
7	634.02	2389.06	469.07	− 1187.12	− 1037	1.00
8	963.76	2716.64	634.02	− 1349.90	− 1037	1.00
9	1458.31	3044.22	963.76	− 1512.67	− 1037	1.00
10	2117.66	3371.79	1458.31	− 1675.44	− 1037	1.00
11	2941.81	3699.37	2117.66	− 1838.21	− 1037	1.00
12	3930.77	4026.94	2941.81	− 2000.98	− 1037	1.00
13	5084.54	4354.52	3930.77	− 2163.76	− 1037	1.00
14	6403.10	4682.10	5084.54	− 2326.53	− 1037	1.00
15	7886.47	5009.67	6403.10	− 2489.30	− 1037	1.00
16	9534.65	5337.25	7886.47	− 2652.07	− 1037	1.00
17	5578.49	1940.96	7683.21	− 3139.69	− 906	0.81
18	3661.94	1636.26	5578.49	− 2646.80	− 906	1.00
19	2149.16	982.51	3661.94	− 1589.30	− 906	1.00
20	1040.89	327.50	2149.16	− 529.77	− 906	1.00

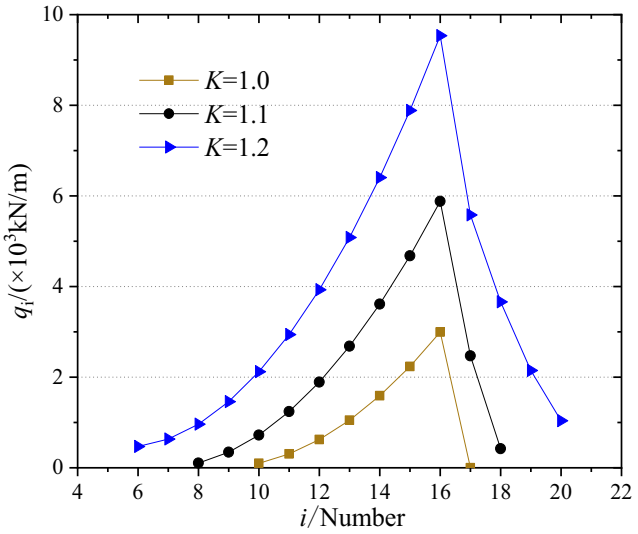

Fig. 3 Relationship between landslide thrust sliding force and safety coefficient

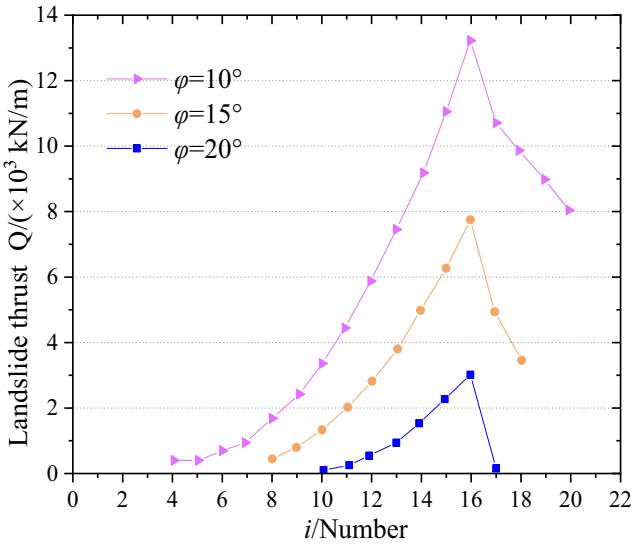

Fig. 5 Relationship between landslide thrust sliding force and internal friction angle

this study. The position relationship between tunnel and landslide is shown in Fig. 7. The section OA of tunnel is within the body of the landslide, and the section AB is within the sliding bed. The underlying immovable rock and soil to which a landslide is attached during sliding is referred to as sliding bed.

The simplified force model is shown in Fig. 8. The parameter q_i is the landslide thrust sliding force, which is calculated by the Eq. (1). The point O is the midpoint of the tunnel model, the part OA is the length of the tunnel within the landslide, and the part AB is the length of the tunnel within the sliding bed. The model is in accordance with the mechanical condition of Winkler's assumption. Since the normal foundation coefficient of the soil around AB tunnel is greater than that around OA tunnel, the stable soil around the tunnel within the sliding bed has "anchoring" effect on the tunnel within the landslide. If the length of tunnel AB is long enough, its displacement will approach zero at a certain position.

Taking the i-th unit in the axial direction of the tunnel for force analysis, as shown in Fig. 9, the parameter ω_{i-1}^R is the deflection on the right side of unit i-1, M_{i-1}^R is the bending moment on the right side of unit i-1, ϕ_{i-1}^R is the rotation angle on the right side of unit i-1, and Q_{i-1}^R is the shear force on the right side of unit i-1, ω_i^L is the deflection on the left side of unit i, M_i^L is the bending moment on the left side of unit i, ϕ_i^L is the rotation angle on the left side of unit i, and Q_i^L is the shear force on the left side of unit i. The superscripts L and R of the parameters in all formulas mean the left and right sides of the unit respectively.

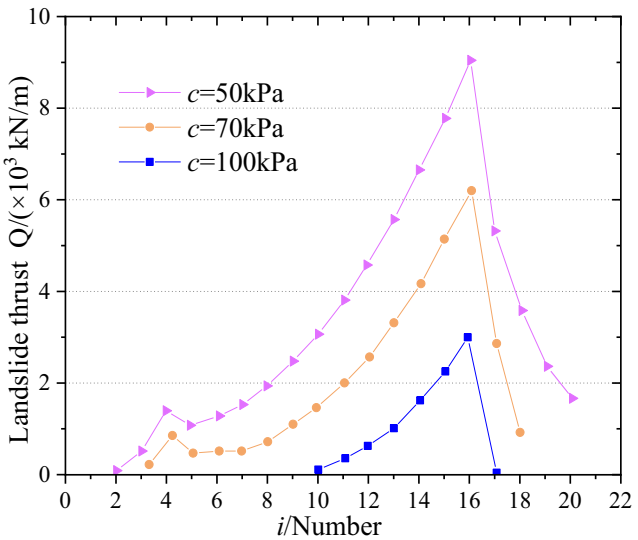

Fig. 4 Relationship between landslide thrust sliding force and cohesive force

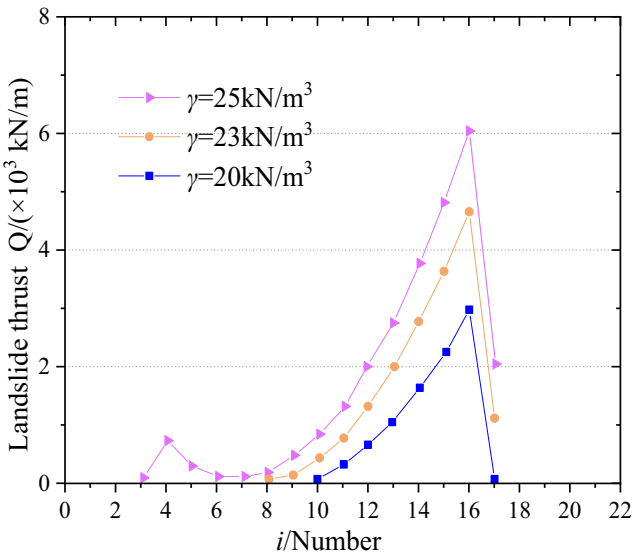

Fig. 6 Relationship between landslide thrust sliding force and landslide unit weight

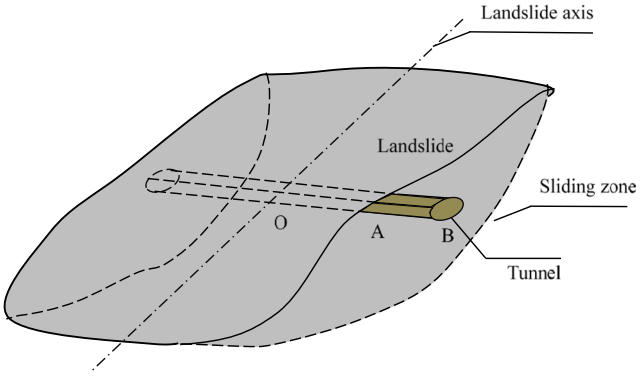

Fig. 7 Tunnel axial crossing vertical to sliding direction of landslide

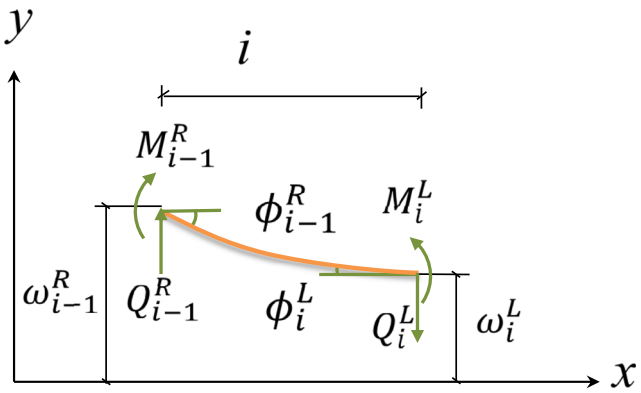

Fig. 9 Force analysis for *i* unit

According to the stress balance condition, the equilibrium equation can be obtained as follows:

$$Q_i^L - Q_{i-1}^R = 0 \tag{7}$$

$$M_i^L - M_{i-1}^R - Q_{i-1}^R L_i = 0 \tag{8}$$

$$\omega_i^L = \omega_{i-1}^R - \phi_{i-1}^R L_i - M_i^L \cdot \frac{L_i^2}{2EI_i} + Q_i^L \cdot \frac{L_i^3}{3EI_i} \tag{9}$$

$$\phi_i^L = \phi_{i-1}^R + M_i^L \frac{L_i}{EI_i} - Q_i^L \frac{L_i^2}{2EI_i} \tag{10}$$

Combining the expressions in above equations leads to:

$$\left[S_i^L\right] = \begin{bmatrix} 1 \\ Q_i^L \\ M_i^L \\ \omega_i^L \\ \phi_i^L \end{bmatrix} = \begin{bmatrix} 1 & 0 & 0 & 0 & 0 \\ 0 & 1 & 0 & 0 & 0 \\ 0 & L_i & 1 & 0 & 0 \\ 0 & -\frac{L_i^3}{6EI_i} & -\frac{L_i^2}{2EI_i} & 1 & -L_i \\ 0 & \frac{L_i^2}{2EI_i} & \frac{L_i}{EI_i} & 0 & 1 \end{bmatrix} \begin{bmatrix} 1 \\ Q_{i-1}^R \\ M_{i-1}^R \\ \omega_{i-1}^R \\ \phi_{i-1}^R \end{bmatrix} = \left[D_{i,i-1}\right]\left[S_{i-1}^R\right] \tag{11}$$

where $\left[S_i^L\right]$ is the internal force matrix on the left side of unit *i*,, $[D_{i,\,i-1}]$ is the transfer matrix from the right side of the unit *i*-1 to the left side of the unit *i*, $\left[S_{i-1}^R\right]$ is the internal force matrix from the right side of the unit *i*-1, EI_i is the flexural rigidity, and L_i is the tunnel length.

The internal force of the *i*-th node is analyzed by Fig. 10. In the figure, Q_i^R, M_i^R, ω_i^R, and ϕ_i^R are the shear force, bending moment, deflection, and rotation angle of the right side of the unit *i*, respectively. Q_i^L, M_i^L, ω_i^L, and ϕ_i^L are the shearing force, bending moment, deflection, and rotation angle of the left side of the unit *i*, respectively.

The matrix equation can be derived from the equilibrium condition:

$$\left[S_i^R\right] = \begin{bmatrix} 1 \\ Q_i^R \\ M_i^R \\ \omega_i^R \\ \phi_i^R \end{bmatrix} = \begin{bmatrix} 1 & 0 & 0 & 0 & 0 \\ -q_i & 1 & 0 & k_i & 0 \\ M_i & 0 & 1 & 0 & 0 \\ 0 & 0 & 0 & 1 & 0 \\ 0 & 0 & 0 & 0 & 1 \end{bmatrix} \begin{bmatrix} 1 \\ Q_i^L \\ M_i^L \\ \omega_i^L \\ \phi_i^L \end{bmatrix} = [G_i]\left[S_i^L\right] \tag{12}$$

where $\left[S_i^R\right]$ is the internal force matrix on the right side of unit *i*; $[G_i]$ is the transfer matrix of the internal forces on the left and right sides of unit *i*; $\left[S_i^L\right]$ is the internal force matrix on the left side of unit *i*, k_i is the foundation coefficient (Vesic 1961); q_i is the landslide thrust force calculated by Eq. (1).

$$k_i = \frac{0.65E_S}{B(1-\nu^2)} \sqrt[12]{\frac{E_S B^4}{EI}} \tag{13}$$

where E_s is the elastic modulus of the soil; ν is Poisson's ratio of the soil; *EI* is the bending stiffness of the beam; *B* is the width of the beam (in this paper, it is the outer diameter of the tunnel).

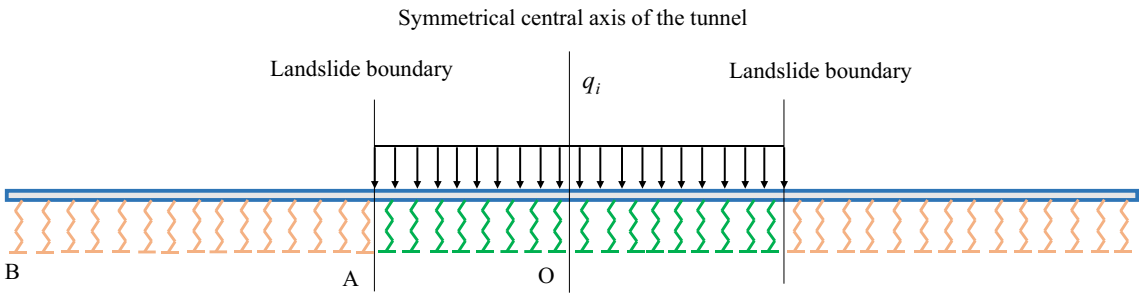

Fig. 8 Simplified foundation beam model of tunnel landslide

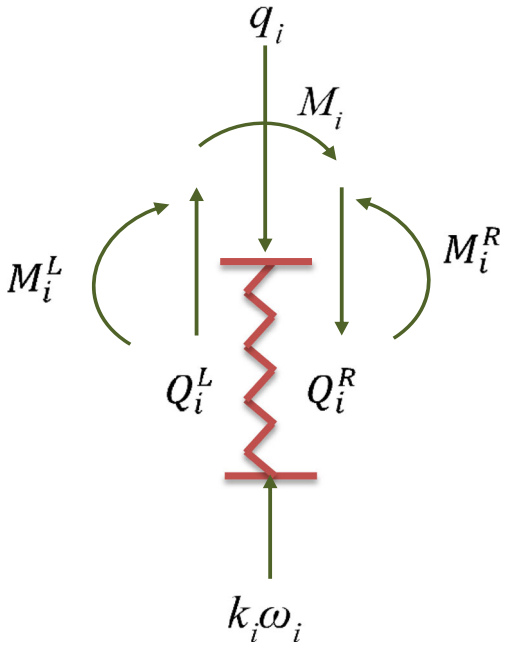

Fig. 10 Internal force transfer of *i* unit

Substituting Eq. (12) into Eq. (11), the internal force matrix on the left side of unit *n* can be obtained:

$$S_n^L = [D_{n,n-1}][G_{n-1}]\cdots\cdots[G_i][D_{i,i-1}]\cdots\cdots[G_2][D_{2,1}][G_1][D_{1,0}][S_0^R] \tag{14}$$

Equation (14) can be solved by combining the boundary conditions.

For the foundation model shown in Fig. 8, the boundary conditions are:

$$[Q_O \ \ \phi_O]^{\mathrm{T}} = [0 \quad 0]^{\mathrm{T}}, \quad [\omega_B \quad \phi_B] = [0 \quad 0]^{\mathrm{T}} \tag{15}$$

There are four equations and eight unknowns in Eq. (14) and there are four boundary conditions in Eq. (15). Through combining Eqs. (14) and (15), a total of eight equations and eight unknowns can be obtained, and all unknowns can be solved. After calculating the unknown $[S_0^R]$, the transfer matrix method can be used to solve all the remaining unknowns. The equations are listed as follows:

$$[S_1^{\mathrm{L}}] = [D_{1,0}][S_0^{\mathrm{R}}] \tag{16}$$

$$[S_1^{\mathrm{R}}] = [G_1][S_1^{\mathrm{L}}] \tag{17}$$

$$[S_i^{\mathrm{L}}] = [D_{i,i-1}][S_{i-1}^{\mathrm{R}}] \tag{18}$$

$$[S_i^{\mathrm{R}}] = [D_i][S_i^{\mathrm{L}}] \tag{19}$$

Finally, the internal forces and deformation of any section of the tunnel structure can be obtained considering the effects of the landslides.

Case analyses

The model geometry parameters are as follows: The total length of the tunnel is 170 m. The length of tunnel in landslide is 50 m. The length of the tunnel within the landslide is 120 m in total, of which 60 m on each side of the landslide. The outer diameter of the tunnel is 6.68 m, the tunnel thickness is 0.48 m, and the tunnel cross-section area is 19.52 m^2. The calculating parameters are as follows: the elastic modulus E is set as 6.5×10^4 MPa, the inertia moment I is set as 11.80 m^4, the bending stiffness EI is 7.67×10^8 kN·m^2. The foundation coefficient of landslide is k_{ibody}; the foundation coefficient of the sliding bed is k_{ibed}; the landslide thrust sliding force acting on the tunnel within the landslide is q. From Eq. (13) and the above related parameters, k_{ibody}, k_{ibed} and q can be calculated. We can get $k_{\mathrm{ibody}} = 9.09 \times 10^4$ kN/m^3, $k_{\mathrm{ibed}} = 2.91 \times 10^5$ kN/m^3, and $q = 500$ kN/m.

During the calculation process, the tunnel is divided into 170 elements, that is, per meter is divided into one unit. Since the calculation model is symmetrical, it can only be analyzed on the left side. The internal force and deformation for the existing tunnels are shown in Fig. 11.

Figure 11 a shows that the maximum for the bending moment appears near the landslide boundary $x = -5$ m under the action of landslide thrust sliding force. It is noteworthy that the distribution of tunnel bending moment in the sliding bed is from negative to positive value. Finally, it is reduced to zero and the influence depth is about 50 m. In the middle of the tunnel length, the bending moment is the largest at $x = 25$ m. The bending moment is 0 when x is approximately 3 m. Figure 11b shows the deflection distribution under the effects of the landslide thrust. As shown in Fig. 11b, the deflection is the largest when x is equal to 25 m, and there is also displacement along the landslide boundary. In the sliding bed, the displacement value changes from negative to positive, and it gradually disappears when x is near to -50 m. Figure 11c is a shear diagram under the effects of the landslide thrust. As shown in Fig. 11c, there is a sudden change of shear force at the boundary of the landslide, and the shear values on both sides of the landslide are basically equal. On the left side of the landslide boundary, the shear force changes from negative to positive, and on the right side of the landslide boundary, the shear curve approaches a parabola. Figure 11d shows the tunnel rotation angle diagram under the action of landslide thrust sliding force. The rotation angle is the largest near x equals to 0 m, and it approaches zero at $x = 25$ m. In the x range from -35 to -20 m, the tunnel has reverse warping. In this figure and subsequent tunnel internal force deformation figure, the area with green background color is the area of the sliding bed, and the area with yellow background color is the landslide area.

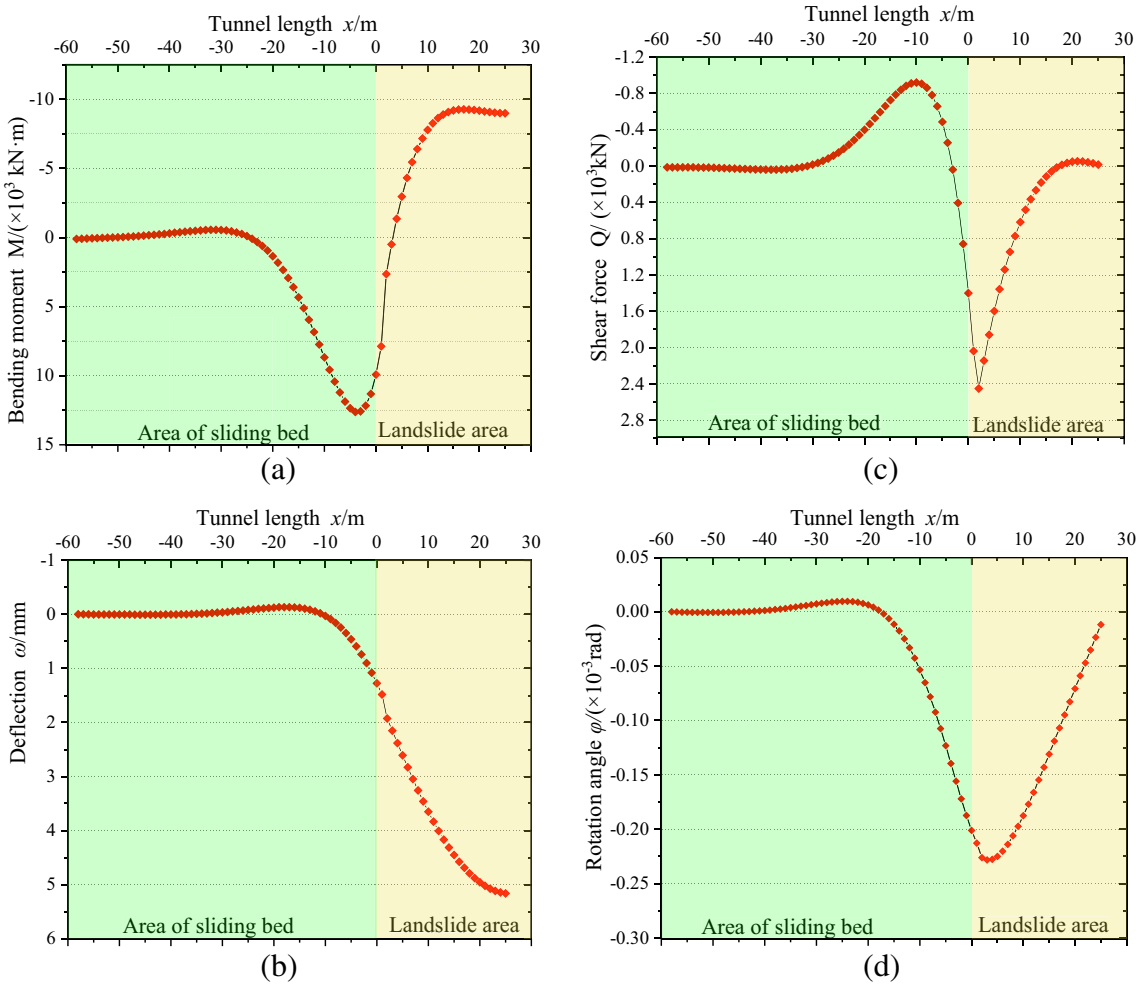

Fig. 11 Internal force and deflection for tunnel. **a** Bending moment curve for tunnel. **b** Deflection curve for tunnel. **c** Shear force curve for tunnel. **d** Rotation angle curve for tunnel

Example verification

Numerical simulation analyses

In order to verify the effectiveness and applicability of the simplified analytical solution in this study, the numerical simulation method is used and the element discrete model is shown in Fig. 12. The size of the model is from 0 to 175 m in the direction *z*, from 0 to 300 m in the direction *x,* and from 0 to 187.5 m in the direction *y,* respectively. The coordinate *xyz* and origin are shown in Fig. 12. As shown in Fig. 12, the model consists of five parts: the sliding bed, the landslide, the sliding zone, the lining in sliding bed and in landslide, which are distinguished by different colors. The number of meshes and nodes is 279900 and 293112, respectively. The excavation of the tunnel is realized by setting the "group" of the tunnel as "null".

The physical parameters of this model are selected in Table 5. The numerical simulation conditions are listed as follows: (1) The displacement constraint condition are: Fixed the *z*-direction displacement of all nodes, fixed the *x, y, z*-direction displacement of all nodes in the plane where y equals 0 m, and fixed the *x*-direction displacement of all nodes in the planes where *x* equals 0 and 300 m. (2) The Mohr-Coulomb criterion is used for the sliding bed, the landslide, and the sliding zone, and the elastic criterion is used in the lining. The initial in situ stress is gravity stress field and the gravity direction is -y. (3) The initial in situ stress is balanced first, and then the displacement of all nodes is set to zero to ensure that the calculation is based on the initial in-situ stress balance state.

In this study, the numerical simulation results for the tunnel-landslide interaction are extracted, including the total displacement, the Y-direction displacement, the X-direction displacement, and the principal stress. Figure 13 shows the total displacement nephogram of the existing tunnel caused by the landslide. From the figure, it can be seen that the displacement of the tunnel within the sliding bed is basically zero, and the tunnel within the landslide has deformation along the sliding direction under the thrust of the landslide.

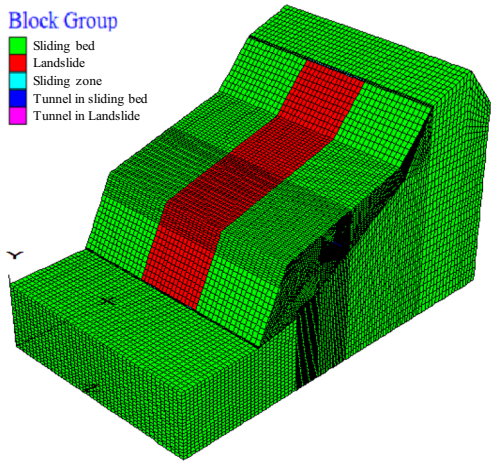

(a)

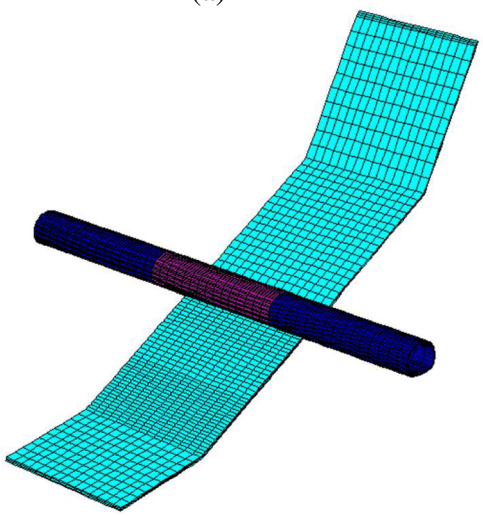

(b)

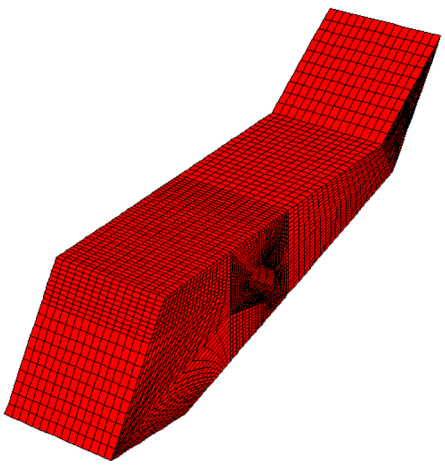

(c)

Fig. 12 Numerical model. **a** Tunnel-landslide overall model. **b** Lining and sliding zone. **c** Landslide model

The maximum displacement is about 10 mm. Figures 14 and 15 show the displacement rules of the tunnel in the Y and X direction, respectively. It can be seen that there is almost no displacement of the tunnel within the sliding bed, and the displacement of middle tunnel within the landslide is the largest, and gradually decreases to both sides. Figure 16 is the principal stress of the tunnel due to landslide. It shows in the figure that the principal stress of the tunnel at the junction of landslide and sliding bed is the largest and gradually decreases to both sides. Figures 17 and 18 are stress nephograms in Y and X directions of the tunnel, respectively. The stress of the tunnel within the landslide is larger value and gradually decreases to both sides.

Comparison of numerical and simplified analytical solution

The deflection comparison between the numerical solution and the simplified analytical solution is shown in Fig. 19. The range of x greater than − 60 m and less than 0 m is the length range of the tunnel in the sliding bed, and the range of x greater than 0 m and less than 25 m is the length range of the tunnel in the landslide. The figure shows that the trends of both simplified analytical and numerical solution are very similar. When x is within the range of − 30 to − 10 m, the calculated result of the numerical solution is slightly larger than that of the simplified analytical solution. When x is within the range of 10 to 20 m, the calculated result of the numerical solution is slightly smaller than that of the simplified analytical solution. For x = 25 m, both the numerical solution and the simplified analytical solution reach the maximum value, about 10 mm.

Comparison of the bending moments between the numerical and simplified analytical solution is shown in Fig. 20. The range of x greater than − 60 m and less than 0 m is the length range of the tunnel in the sliding bed, and the range of x greater than 0 m and less than 25 m is the length range of the tunnel in the landslide. When x is within the range of − 20 to − 5 m, the calculated result of the numerical solution is larger than that of the simplified analytical solution. When x is within the range of 0 to 10 m, the calculated result of the numerical solution is slightly smaller than that of the simplified analytical solution. When x is within the range of 10 to 25 m, the calculated result of the numerical solution is slightly larger than that of the simplified analytical solution. At a position where x is equal to − 5 m, the bending moment reaches a maximum value of about 2.0×10^4 kN·m. Generally speaking, the simplified analytical solution is in good agreement with the numerical values.

Analyses of influence parameters

In order to further understand the interaction mechanism between tunnel and landslide, the influence parameters are

Table 5 Physical parameters of numerical model

Name	Cohesion (MPa)	Internal friction angle (°)	Weight (kN/m^3)	Elastic Modulus (MPa)	Poisson's ratio
Sliding bed	0.5	39	23	2000	0.28
Landslide	0.1	35	20	800	0.30
sliding zone	0.015	33	20	200	0.32
Lining in sliding bed Lining in tlandslide	–	–	25	2.5e4	0.223

analyzed in this study. The total length of the tunnel is 170 m. Among them, the length of the tunnel in the landslide is 50 m; the length of the tunnel in the sliding bed is 120 m, and the two sides of the landslide account for 60 m. The elastic modulus E is set as 6.5×10^4 MPa, the inertia moment I is set as 11.80 m^4, so the bending stiffness EI is 7.67×10^8kN·m^2. The outer diameter of the tunnel is 6.68 m, the thickness is 0.48 m, and the cross-section area is 19.52 m^2.

Influence of landslide thrust sliding force on internal force and deflection of tunnel

Setting parameters are as follows: k_{ibody} defined as the foundation coefficient of the landslide is 4.0×10^4 kN/m^3; k_{ibed} defined as the foundation coefficient of the sliding bed is 5.0×10^5 kN/m^3; q defined as the landslide thrust sliding force acting on the tunnel within the landslide is taken as 200 kN/m, 500 kN/m, and 800 kN/m, respectively. The internal force and displacement curves for the existing tunnel induced by the landslide thrust sliding force are shown in Fig. 21.

As shown in Fig. 21a, at the same location of the tunnel, the bending moment increases gradually with the increase of the tunnel load. At the junction of landslide and sliding bed (near the left side of x equal to 0), the bending moment values are about 1.0×10^4 kN·m, 2.5×10^4 kN·m, and 4.0×10^4 kN·m, respectively. In the middle of the tunnel (x equals about 25 m), the bending moment values are about 1.0×10^4 kN·m, 2.0×10^4 kN·m, and 4.0×10^4 kN·m, respectively. Figure 21b shows the deflection distribution of tunnels under different landslide thrust sliding forces. From the figure, it can be seen that the deflection increases gradually with the increase of loads, and the deflection is the largest in the middle of the tunnel location. The maximum deflections under different loads are about 4 mm, 10 mm, and 17 mm, respectively. Within the sliding bed, when x is within the range of − 30 to − 10 m, the tunnel has reverse displacement. Figure 21c shows the shear curves of tunnels under different landslide thrust sliding forces. In general, the shear force increases gradually with the increase of landslide thrust sliding force. At the junction of landslide and sliding bed (x equals about 0), the shear force on the left side is less than that on the right side; the shear force on the right side is about 2×10^3 kN, 4×10^3 kN, and 7×10^3 kN, respectively. Figure 21d shows the tunnel rotation angle curves under different landslide thrust sliding forces. The rotation angle of the tunnel increases with the increase of the landslide thrust sliding force. When x is in the range of − 30 to − 20 m, the tunnel has different degrees of reverse bending. Furthermore, the greater the load is, the more obvious the reverse bending of the tunnel is. Under different landslide thrust sliding forces, the rotation angles near x = 5 m are 0.2×10^{-3} rad, 0.45×10^{-3} rad, and 0.75×10^{-3} rad, respectively. The rotation angle at x = 25 m is reduced to zero.

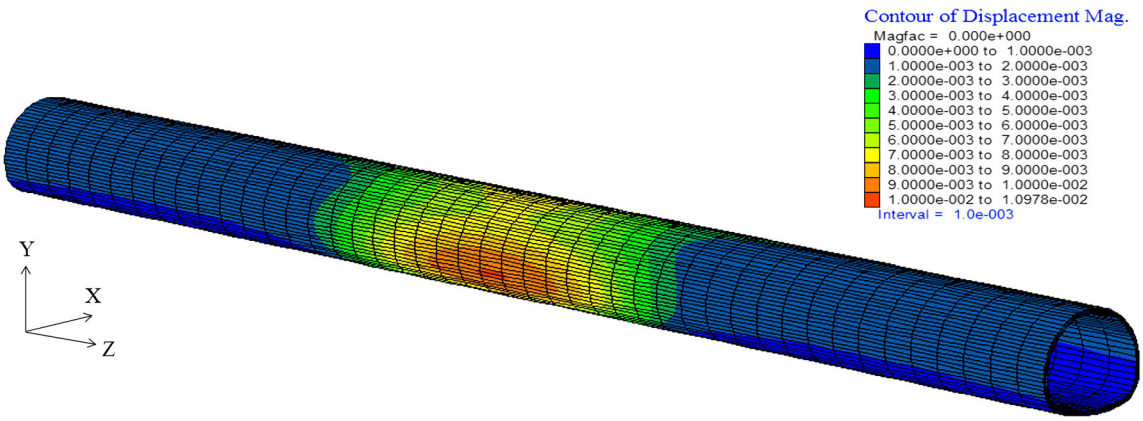

Fig. 13 Tunnel displacement nephogram

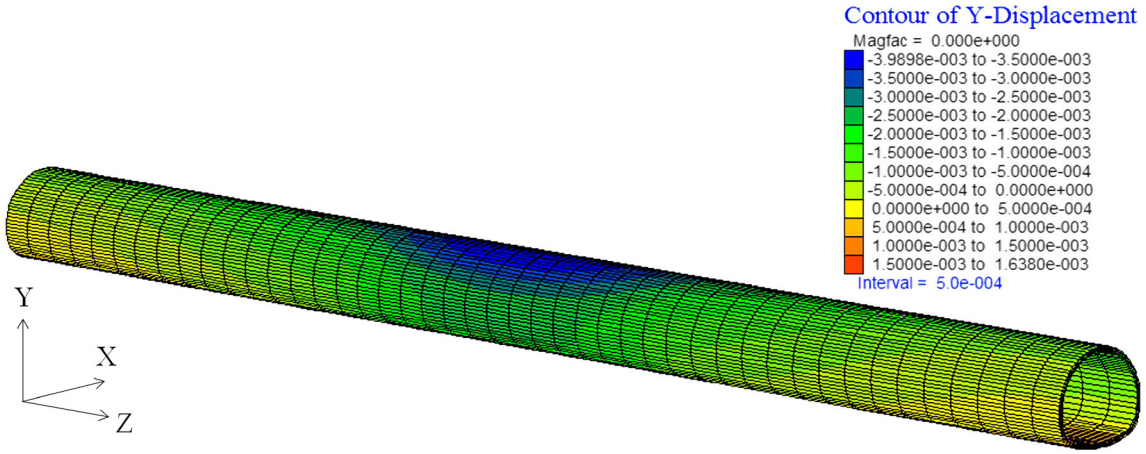

Fig. 14 Y-direction tunnel displacement nephogram

Influence of foundation coefficient of landslide on internal force and deflection of tunnel

Setting parameters are as follows: k_{ibed} defined as the foundation coefficient of the sliding bed is 5.0×10^5 kN/m^3; q defined as the landslide thrust sliding force acting on the tunnel within the landslide is 500 kN/m; k_{ibody} defined as the foundation coefficients of the landslide are taken as 4.0×10^4 kN/m^3, 7.0×10^4 kN/m^3, and 1.0×10^5 kN/m^3, respectively. Figure 22 shows the internal force and deflection curves of the tunnel with different foundation coefficient of the landslide.

As shown in Fig. 22a, as the foundation coefficient of the landslide increases, the maximum bending moment gradually decreases. At the junction of the tunnel and the landslide (x equals about − 5 m), the bending moment values are about 1.0×10^4 kN·m, 2.0×10^4 kN·m, and 4.0×10^4 kN·m, respectively. In the middle of the tunnel (x equals about 25 m), the bending moment values are about 2.0×10^4 kN·m, 1.0×10^4 kN·m, and 0.75×10^4 kN·m, respectively. The bending moment is zero when x equal to 5 m. It can be seen from Fig. 22b that the deflection is the largest in the middle of the tunnel, and the deflection gradually decreases as the foundation coefficient of the landslide increases. Under different landslide foundation coefficients, the deflections are about 5 mm, 7 mm, and 11 mm at x equal to 25 m, respectively; the deflection at the junction of the landslide tunnel (x is equal to 0) is about 2 mm, 3 mm, and 4 mm, respectively. In the range of x from – 30 to – 10 m, there is substantially no deflection. It shows from Fig. 22c that as the coefficient of the foundation of landslide increases, the shear force gradually decreases. In the vicinity of the right side where x is equal to zero, the shear forces for three cases reach to maximum value, which are about 2.5×10^3 kN, 3.0×10^3 kN, and 4.5×10^3 kN, respectively. At a position where x is equal to − 25 m and x is equal to 25 m, the shear force is substantially reduced to zero. Figure 22d shows the rotation angle curves with different foundation coefficients of the landslide. As the foundation coefficient of the landslide increases, the rotation angle of the tunnel gradually decreases. In the vicinity of $x = 5$ m, the rotation angles of the tunnel are 0.45×10^{-3} rad,

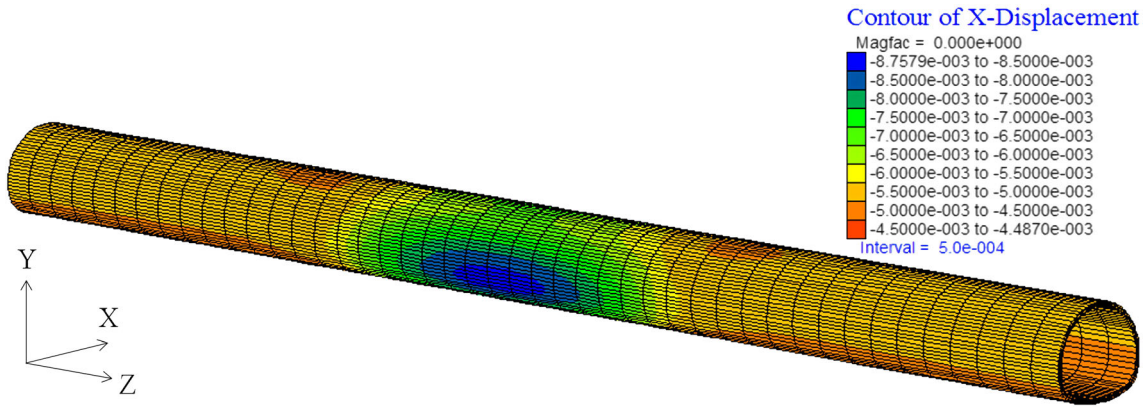

Fig. 15 X-direction tunnel displacement nephogram

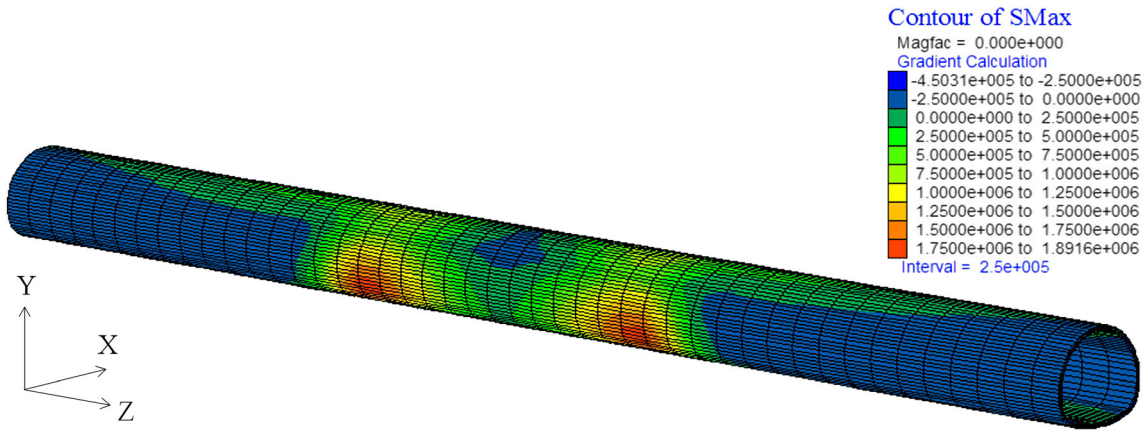

Fig. 16 Tunnel principal stress nephogram

0.3×10^{-3} rad, and 0.25×10^{-3} rad, respectively. In the middle of the tunnel (where x equals 25 m), the rotation angle is reduced to 0. When x is in the range of − 35 to − 20 m, the tunnel has reverse bending moment.

Influence of foundation coefficient of sliding bed on internal force and deflection of tunnel

Setting parameters are as follows: k_{ibody} defined as the foundation coefficient of the landslide is 4.0×10^4 kN/m^3; q defined as the landslide thrust sliding force acting on the tunnel within the landslide is 500 kN/m; k_{ibed} defined as the foundation coefficient of the sliding bed is taken as 5.0×10^5 kN/m^3, 1.0×10^6 kN/m^3, and 1.5×10^6 kN/m^3, respectively.

Figure 23 shows the internal force and deflection curves of the tunnel with different foundation coefficient of sliding bed. As shown in Fig. 23a that as the foundation coefficient of sliding bed increases, the bending moment gradually increases. The bending moments for three cases reach to the largest at the junction of the landslide and the sliding bed, which are 2.5 × 104 kN·m, 3.0 × 104 kN·m, and 3.5 × 104 kN·m, respectively. In the middle of the tunnel, the bending moments are basically the same, both around 2.5×10^4 kN·m. Figure 23b are tunnel deflection curves under different sliding bed foundation coefficients. Generally speaking, the variation of sliding bed foundation coefficients has little effect on tunnel deflection. The deflection of the middle part of the tunnel (where x equals 25 m) is the largest, and it is about 10 mm in all three cases. When x equals zero, the deflection of the tunnel is about 2 mm in all three cases. Figure 23c is a tunnel shear diagram with different foundation coefficients of sliding bed. The shear force on both sides of the boundary between landslide and sliding bed is the largest. Near the right side where x equals 0, the shear force is about 5.0×10^3 kN. Near the left side where x equals zero, the shear forces are about 2×10^3 kN, 4×10^3 kN, and 7×10^3 kN, respectively. The shear force on both sides of x equals 0 decreases gradually. In the middle of the tunnel (where x equals 25 m), the shear force is

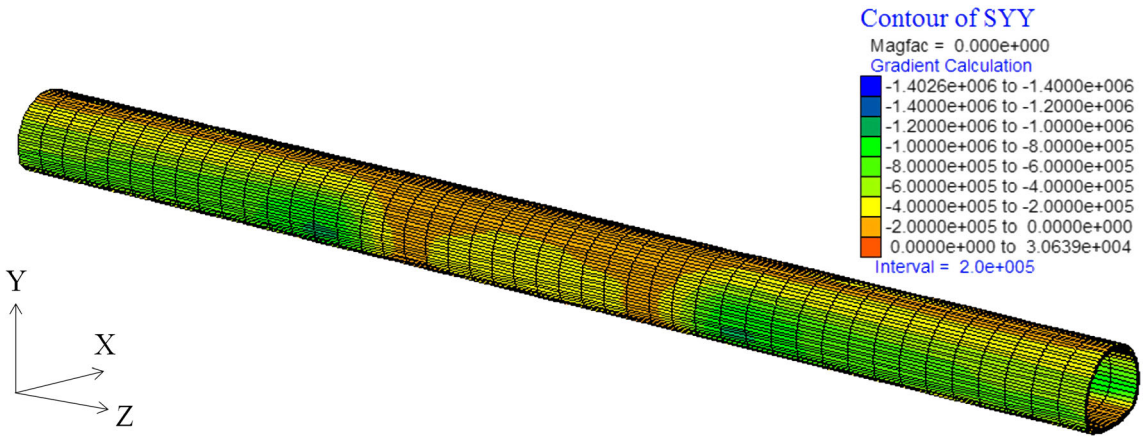

Fig. 17 Y-direction tunnel stress nephogram

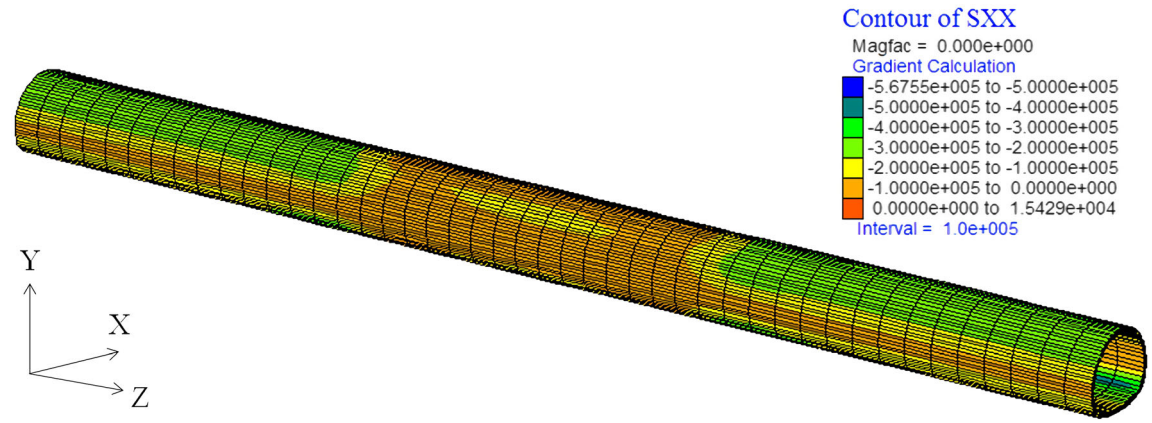

Fig. 18 X-direction tunnel stress nephogram

basically zero. Figure 23d shows the tunnel rotation angle diagram with different foundation coefficients of the sliding bed respectively. On the right side where x equals 0, the influence of foundation coefficient of sliding bed on tunnel rotation angle is negligible. When x is about 5 m, the rotation angle of the tunnel is about 0.45×10^{-3} rad. When x is in the range of − 30 to − 15 m, the tunnel has reverse bending.

Influence of tunnel lining stiffness on internal force and deflection of tunnel

Setting parameters are as follows: k_{ibody} defined as the foundation coefficient of the landslide is 4.0×10^4 kN/m^3; k_{ibed} defined as the foundation coefficient of the sliding bed is 5.0×10^5 kN/m^3; q defined as the landslide thrust sliding force acting on the tunnel within the landslide is 500 kN/m. The bending stiffness EI is taken as 4.0×10^8 kN·m^2, 7.67×10^8 kN·m^2, and 1.2×10^9 kN·m^2, respectively. Figure 24 shows the internal force and displacement curves for the tunnel with different lining stiffness.

Figure 24a shows the bending moments of tunnels with different lining stiffness. It can be seen from the figure that the bending moment increases gradually with the increase of tunnel lining stiffness. When x is placed in the range of − 20 to 5 m, there are bending moments on the lower side of the tunnel; when x is placed in the range of − 5 to 0 m, the tunnel is located in the sliding bed, and there are large bending moments in this range. The maximum values for three cases reach to about 1.5×10^4 kN·m, 2.5×10^4 kN·m, and 3.0×10^4 kN·m, respectively. This part is equivalent to the fixed support of the tunnel. It can be seen from Fig. 24b that as the tunnel lining stiffness increases, the maximum displacement gradually decreases. The tunnel has a large deformation in the range

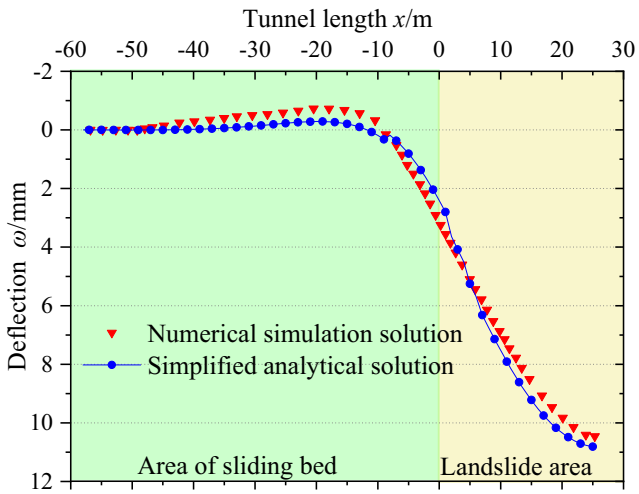

Fig. 19 Comparison of deflection between numerical and simplified analytical solution

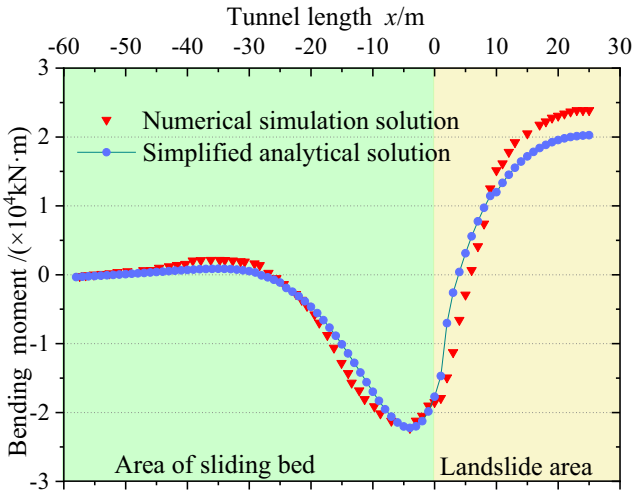

Fig. 20 Comparison of bending moment between numerical and simplified analytical solution

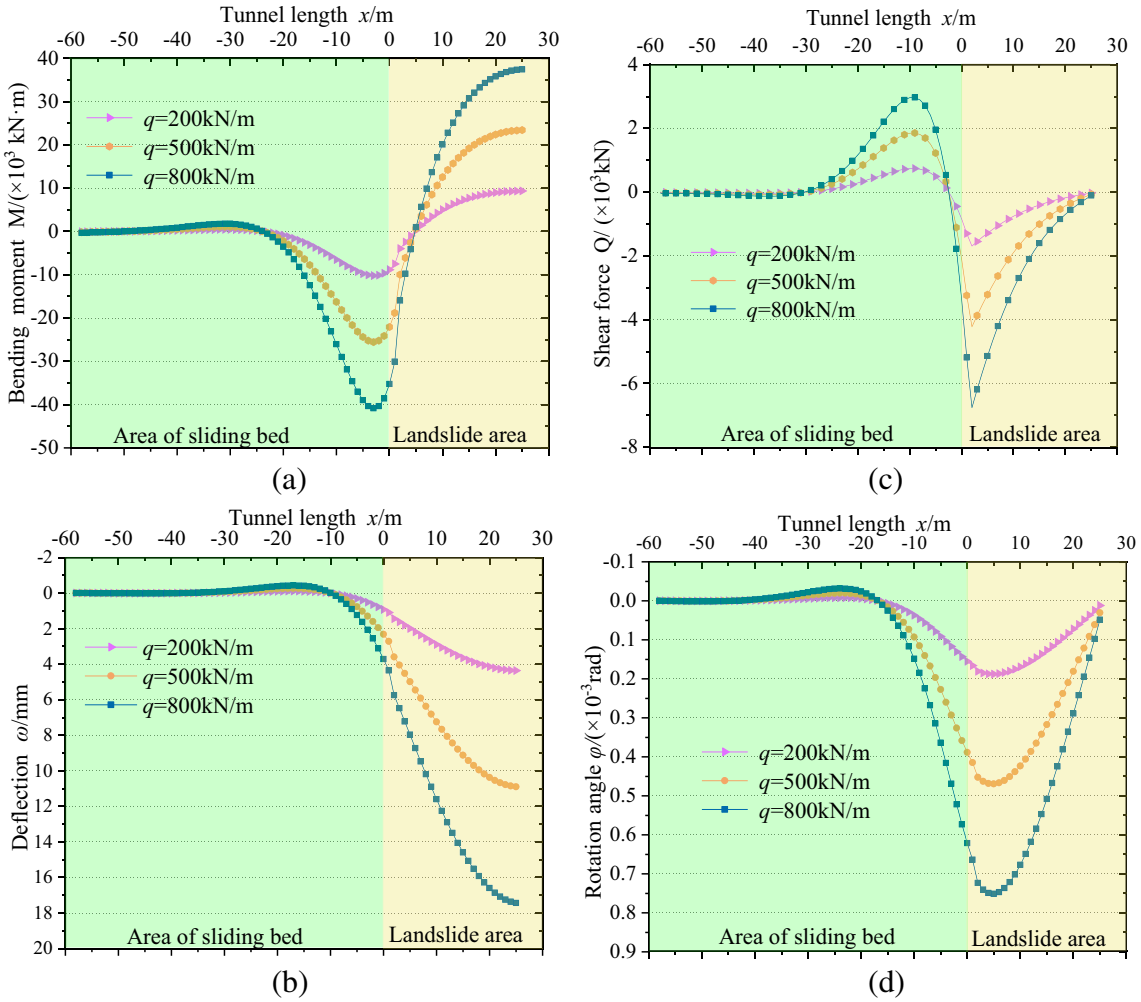

Fig. 21 Internal force and deflection curves for tunnel with different landslide thrust sliding forces. **a** Bending moment curves for tunnel with different landslide thrust sliding forces. **b** Deflection curves for tunnel. **c** Shear force curves for tunnel. **d** Rotation angle curves for tunnel

of − 5 m < x < 30 m, especially in the middle of the tunnel, and the displacements are about 10 mm, 11 mm, and 13 mm respectively. In the range of − 30 m < x < − 10 m, the tunnel has a reverse displacement, mainly because the reaction force of this part of the tunnel is relatively large. Figure 24c shows the shear force curves of the tunnel under different stiffnesses. As the stiffness of the tunnel lining increases, the maximum shear force increases. Near the right side where x equals zero, the shear force of the tunnel is the largest, and the values are about 3.0×10^3 kN, 4.0×10^3 kN, and 5.0×10^3 kN, respectively. In the middle of the tunnel (where x equals 25 m or 30 m), the shear force is basically reduced to zero. Figure 24d is a rotation angle diagram of the tunnel under different stiffnesses. As the stiffness of the tunnel lining increases, the maximum rotation angle gradually decreases. When − 30 m< x <− 25 m, the tunnel has reverse bending. Near x equals 5 m, rotation angles of the tunnel are 0.4×10^{-3} rad, 0.45×10^{-3} rad, and 0.55×10^{-3} rad, respectively. Near x equals 25 m, the rotation angle of the tunnel is reduced to zero.

Influence of tunnel length on internal force and deflection of tunnel

Assume that the length of the tunnel within the landslide is 50 m, 80 m, and 110 m, respectively; the length of the tunnel within the sliding bed is 120 m, of which 60 m on both sides of the landslide. k_{ibody} defined as the foundation coefficient of the landslide is 4.0×10^4

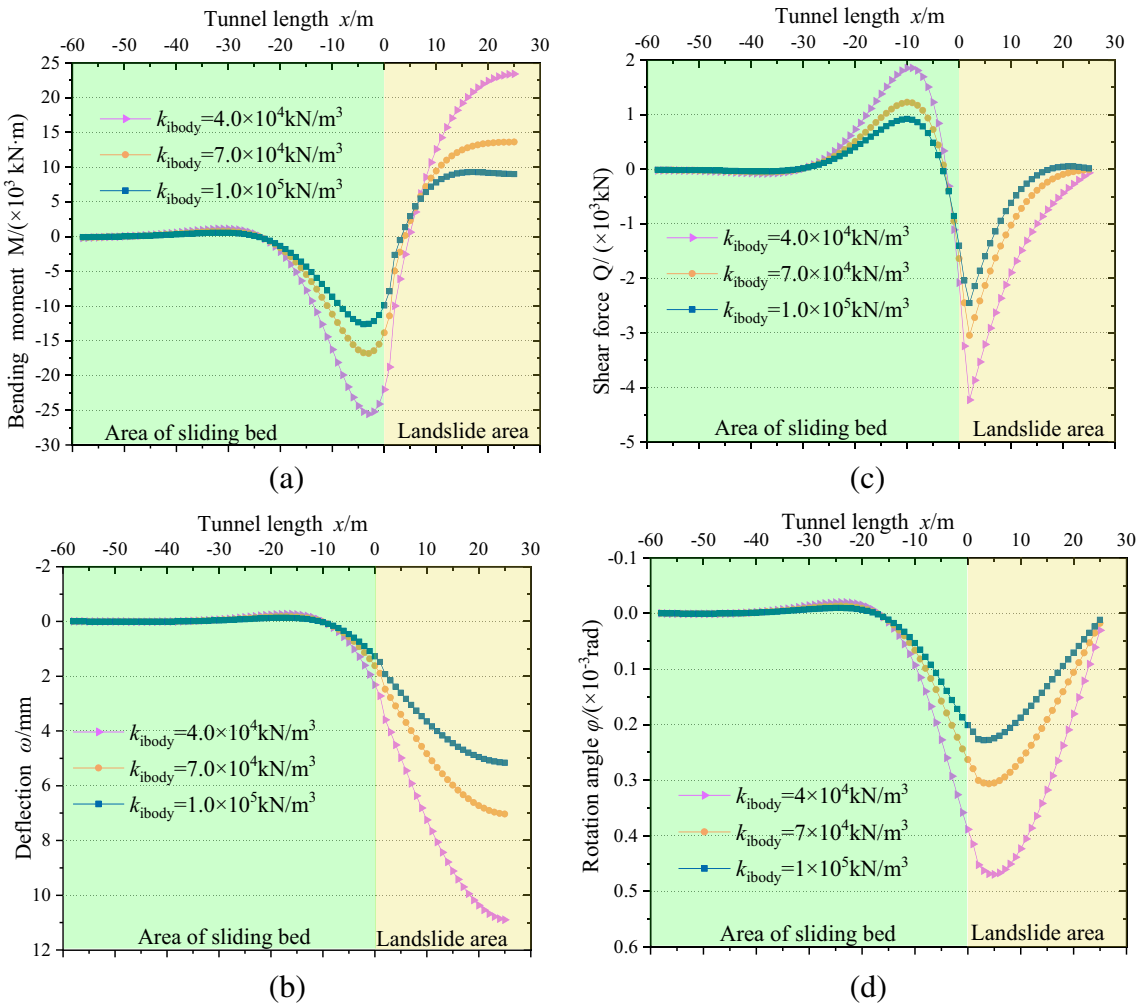

Fig. 22 Internal force and deflection curves for tunnel with different foundation coefficients of landslide. **a** Bending moment curves for tunnel. **b** Deflection curves for tunnel. **c** Shear force curves for tunnel. **d** Rotation angle curves for tunnel

kN/m^3; k_{ibed} defined as the foundation coefficient of the sliding bed is 5.0 × 10^5 kN/m^3; q defined as the landslide thrust sliding force acting on the tunnel within the landslide is 500 kN/m.

Figure 25 shows the internal force and deflection curves of the tunnel when the length of the tunnel within the landslide is 25 m, 40 m, and 55 m respectively. It can be seen from Fig. 25a that when x is in the vicinity of − 5 m, the bending moments are basically the same in three cases; In the middle of the tunnel, the bending moment diagrams of tunnels of different lengths are very different. Especially when the length L of the tunnel in the landslide is equal to 55 m, the bending moment in the middle of the tunnel is basically reduced to zero. When the lengths of the tunnel within the landslide are 25 m and 40 m, the bending moments in the middle of the tunnel are 2.5 × 10^4 kN·m and 1.0 × 10^4 kN·m, respectively. It can be seen from Fig. 25b that the displacement values of tunnels with different lengths in the range of − 60 m < x < 20 m are basically the same, and the maximum displacements appear near the middle of the tunnel, which are about 10 mm, 13 mm, and 12.5 mm respectively. In the range where x is from − 30 to − 10 m, the tunnel has a reverse displacement. It can be seen from Fig. 25c that the tunnel shear force is basically the same in the range of x from − 60 to 0 m; when the tunnel length in the landslide is 25 m, the internal shear force is gradually reduced to 0 when x is greater than zero. The tunnels with lengths L = 40 m and L = 55 m have reverse shear forces in the range of x > 20 m. Figure 25d is a tunnel rotation angle diagram with

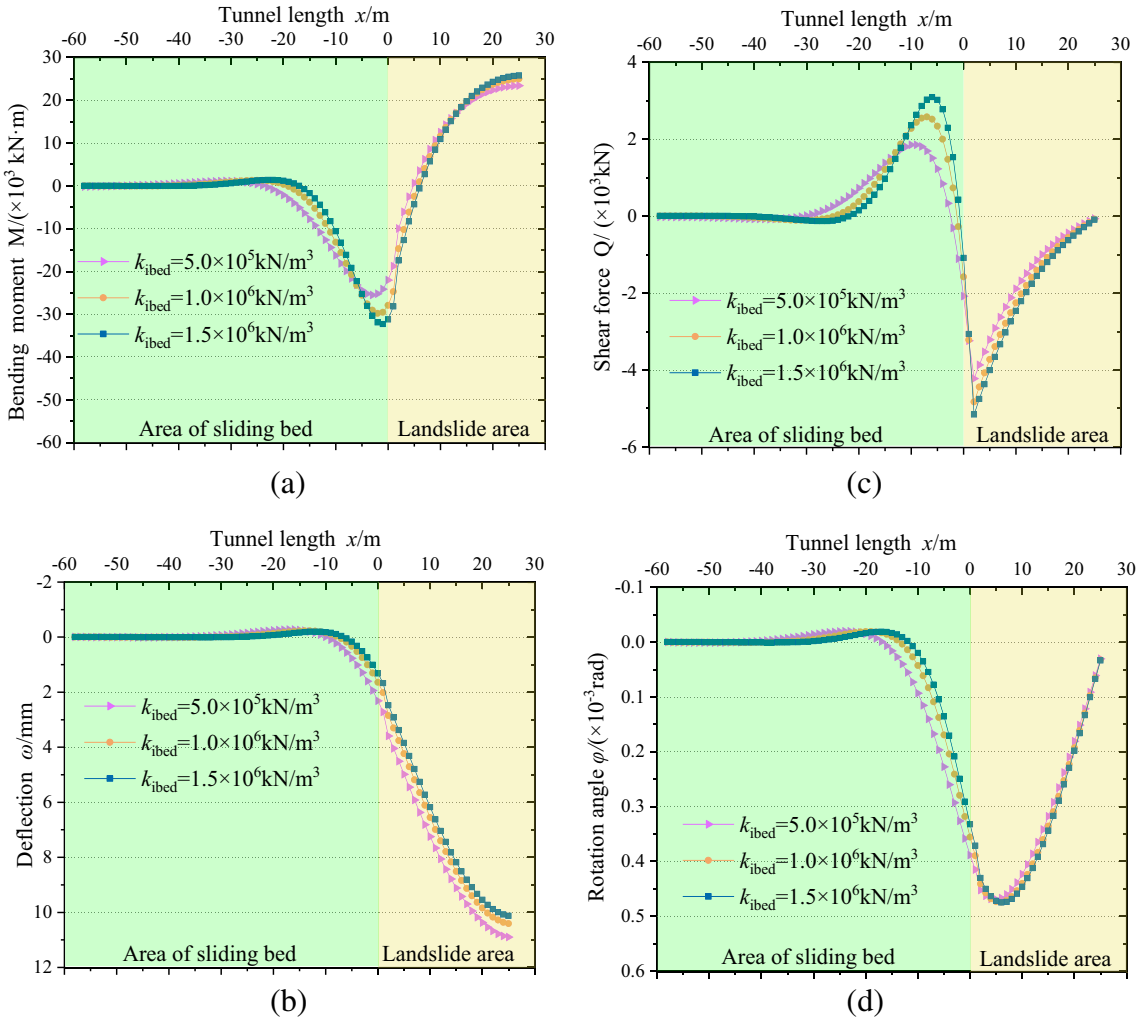

Fig. 23 Internal force and deflection curves for tunnel with different foundation coefficients of sliding bed. **a** Bending moment curves for tunnel. **b** Deflection curves for tunnel. **c** Shear force curves for tunnel. **d** Rotation angle curves for tunnel

different tunnel lengths. It can be seen from the figure that the rotation angle of the tunnel is basically the same in the range of x less than 5 m. The rotation angle of the tunnel is about 0.45×10^{-3} rad in the vicinity of x equals 5 m. In the middle of the tunnel, the rotation angle of the tunnel is basically reduced to zero, but the form of the curve changes is different.

Conclusions

This paper deals with the problem of the influence of mountainous landslides on the deformation of existing tunnels. This study aims to provide theoretical basis for the maintenance and reinforcement of existing tunnels in landslide area. The tunnel model is simplified as an elastic foundation beam, and the interaction between tunnel and landslide is simulated by soil spring. Firstly, based on the transfer coefficient method and the limit equilibrium method, the force balance equation of the landslide is established and the landslide thrust sliding force is obtained. Then, the landslide thrust sliding force is applied to the tunnel structure and the transfer matrix method is used to calculate the tunnel model which has been simplified to elastic foundation beam.

According to the slice method, the tunnel is divided into several parts and the stress of each element is analyzed. Considering the effect of adjacent strip elements, the expression of landslide thrust sliding force is obtained. The influence of the safety coefficient, the cohesive force, and the internal friction angle on the landslide thrust sliding force is analyzed.

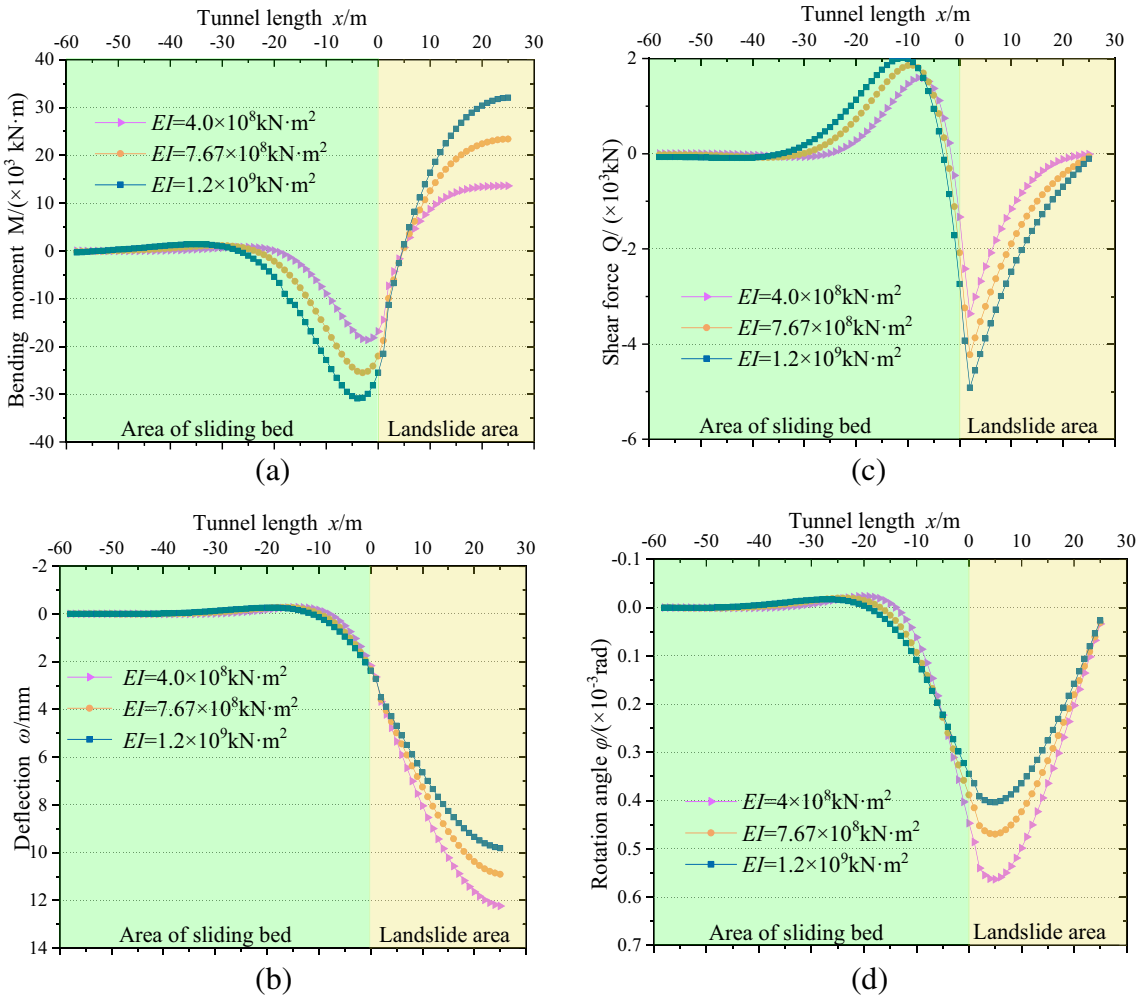

Fig. 24 Internal force and deflection curves for tunnel with different liner stiffness. **a** Bending moment curves for tunnel. **b** Deflection curves for tunnel. **c** Shear force curves for tunnel. **d** Rotation angle curves for tunnel

The results show that with the increase of safety coefficient, the landslide thrust sliding force increases, but the cohesive force and internal friction angle decrease. The internal force and deformation solution of the tunnel are derived by the transfer matrix method. The results show that at the junction between the landslide and the sliding bed and the inside of the landslide, the bending moment of the tunnel is relatively large, and the deformation is the largest in the middle of the tunnel, and the shearing force is abrupt at the junction of the landslide. The internal force and deformation diagram obtained by the simplified analytical solution is compared with the numerical solution. The results show that the numerical solution is basically in agreement with the analytical solution.

The influence of different influence parameters on the internal force and deflection of tunnel is analyzed considering the loads form the landslides. The results show that with the increase of landslide thrust sliding force, the internal force and deflection of tunnel increase gradually. The larger the coefficient of sliding foundation, the smaller the internal force and deflection of tunnel. The coefficient of sliding bed foundation has little influence on the internal force and deflection of tunnel. The greater the stiffness of the tunnel lining, the greater the internal force and the smaller the deflection of the tunnel. Tunnel length has obvious influence on the maximum internal force and deflection of tunnel in landslide, but it has little effect on the internal force and position of tunnel in sliding bed.

It is noteworthy that the major limitation of the proposed method stems from the simplified assumptions of linearity and elasticity. Physically, the landslide soil is perfectly elastic but generally non-linear and tunnel liners are not homogeneous but rather mostly non-homogeneous, but this cannot be

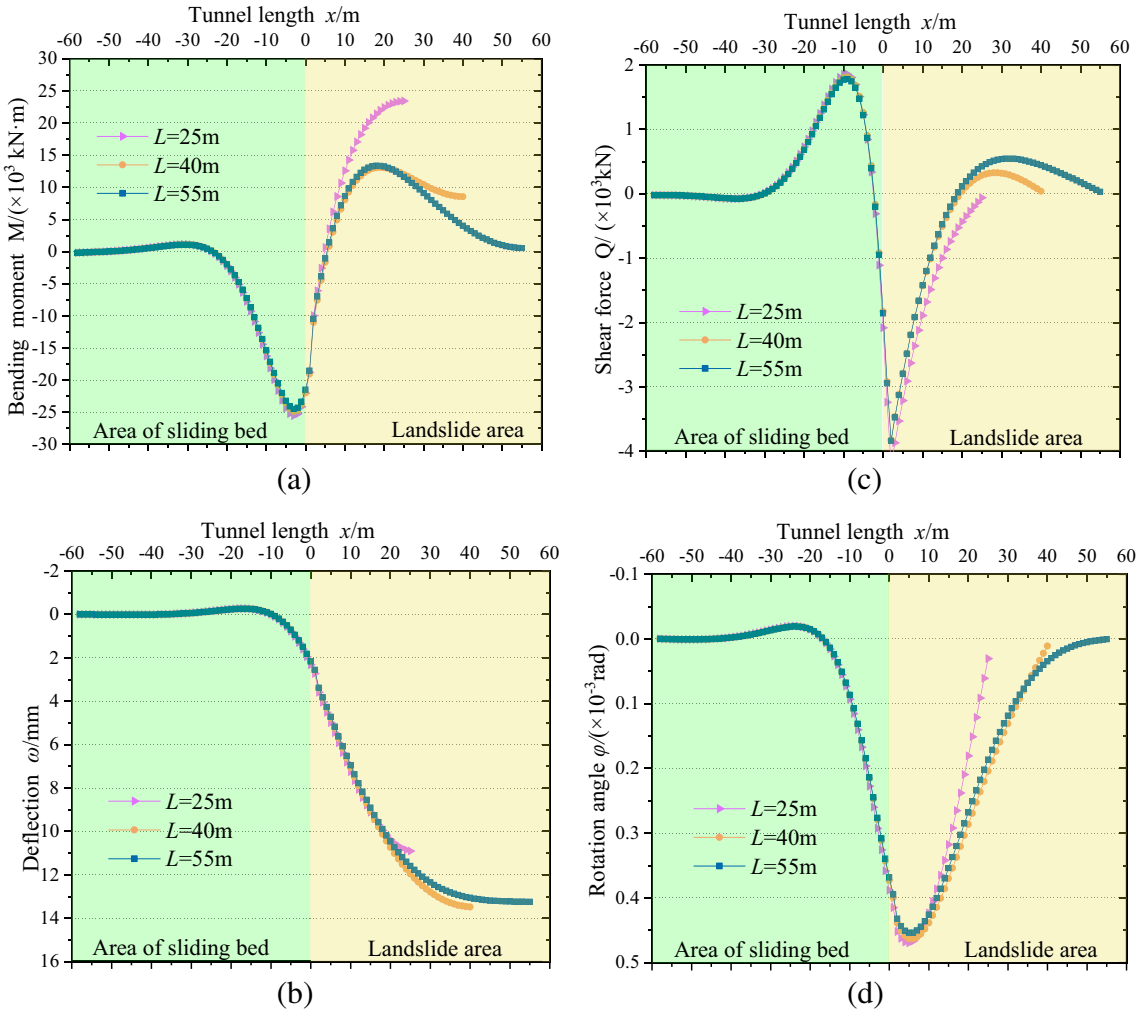

Fig. 25 Internal force and deflection curves for tunnel with different tunnel lengths. **a** Bending moment curves for tunnel. **b** Deflection curves for tunnel. **c** Shear force curves for tunnel. **d** Rotation angle curves for tunnel

considered by this analytical method. Although the range of analytical solutions proposed is limited, it can provide theoretical basis for the maintenance and reinforcement of existing tunnels in landslide area. The complicated response considering advanced mechanisms, such as soil extensive yielding, nonlinear soil behavior, and the elastic-plastic properties of tunnels still require further exploration to approach a solution which conforms with nature. Finally, with the help of numerical software and measure technology, further research remains to be done to assess the influence of landslides on the internal force and the deformation of existing tunnels.

Funding This study received financial support provided by the National Natural Science Foundation of China for General Program (No. 41772331 and 41977247), and the Project of State Key Laboratory Fund for State Key Laboratory of Geohazard Prevention and Geoenvironment Protection (No. SKLGP2015K015), and the Project of Key Laboratory of Geohazard Prevention of Hilly Mountains, Ministry of Natural Resources (Fujian Key Laboratory of Geohazard Prevention, No. FJKLGH2020K004).

Declarations

Competing interests The authors declare no competing interests.

References

Antronico L, Borrelli L, Coscarelli R, Gullà G (2015) Time evolution of landslide damages to buildings: the case study of Lungro (Calabria, Southern Italy). B Eng Geol Environ 74(1):47–59

Bandini A, Berry P, Boldini D (2015) Tunnelling-induced landslides: the Val di Sambro tunnel case study. Eng Geol 196(9):71–87

Barla G (2018) Numerical modeling of deep-seated landslides interacting with man-made structures. J Rock Mech Geotech Eng 10(6):1020–1036

Bayer B, Simoni A, Schmidt D, Bertello L (2017) Using advanced InSAR techniques to monitor landslide deformations induced by tunneling in the Northern Apennines, Italy. Eng Geol 226(8):20–32

Bobet A (2001) Analytical solutions for shallow tunnels in saturated ground. ASCE J Eng Mech 127(12):1258–1266

Casamichele P, Maugeri M, Motta E (2004) Non-linear analysis of soil pipeline interaction in unstable slopes, XIII World Conf. Earthq Eng, Vancouver, Canada

Causse L, Cojean R, Fleurisson JA (2015) Interaction between tunnel and unstable slope-Influence of time-dependent behavior of a tunnel excavation in a deep-seated gravitational slope deformation. Tunn Undergr Space Technol 50(8):270–281

Chiu YC, Lee CH, Wang TT (2017) Lining crack evolution of an operational tunnel influenced by slope instability. Tunn Undergr Space Technol 65(5):167–178

Chou WI, Bobet A (2002) Predictions of ground deformations in shallow tunnels in clay. Tunn Undergr Space Technol 17(1):3–19

Dang HK, Meguid MA (2008) Application of a multilaminate model to simulate the undrained response of structured clay to shield tunnelling. Can Geotech J 45(1):14–28

Do NA, Dias D, Oreste P, Djeran-Maigre I (2014) Three-dimensional numerical simulation of a mechanized twin tunnels in soft ground. Tunn Undergr Space Technol 42(5):40–51

Fang Q, Tai QM, Zhang DL, Wong LNY (2016) Ground surface settlements due to construction of closely-spaced twin tunnels with different geometric arrangements. Tunn Undergr Space Technol 51(1): 144–151

Feng SJ, Gao HY, Gao L, Zhang LM, Chen HX (2019) Numerical modeling of interactions between a flow slide and buildings considering the destruction process. Landslides. https://doi.org/10.1007/s10346-019-01220-9

Friedli B, Hauswirth D, Puzrin AM (2017) Lateral earth pressures in constrained landslides. Géotechnique 67(10):890–905

Fu JY, Yang JS, Yan L, Abbas SM (2015) An analytical solution for deforming twin-parallel tunnels in an elastic half plane. Int J Numer Anal Met 39(5):524–538

Galli A, Di PC (2013) Displacement-based design procedure for slope-stabilizing piles. Can Geotech J 50(1):41–53

Gonzalez C, Sagaseta C (2001) Patterns of soil deformations around tunnels. Application to the extension of Madrid Metro. Comput Geotech 28(6):445–468

Gui MW, Chen SL (2013) Estimation of transverse ground surface settlement induced by DOT shield tunneling. Tunn Undergr Space Technol 33(1):119–130

Hajjar M, Hayati AN, Ahmadi MM, Sadrnejad SA (2015) Longitudinal settlement profile in shallow tunnels in drained conditions. ASCE Int J Geomech 15(6):04014097

Jin DL, Shen X, Yuan DJ (2020) Theoretical analysis of three-dimensional ground displacements induced by shield tunneling. Appl Math Model 79(3):85–105

Koizumi Y, Lee J, Date K, Yokota Y (2010) Numerical analysis of landslide behavior induced by tunnel excavation. Conf. Eur Rock Mech Symp (EUROCK 2010)-Rock Mech Civ Environ Eng, Lausanne, Switzerland

Kong FC, Lu DC, Du XL, Shen CP (2018) Displacement analytical prediction of shallow tunnel based on unified displacement function under slope boundary. Int J Numer Anal Met 43(1):183–211

Lai H, Zhao X, Kang Z, Chen R (2017) A new method for predicting ground settlement caused by twin-tunneling under-crossing an existing tunnel. Environ Earth Sci 76(21):726

Lai J, Wang X, Qiu J, Chen J, Hu Z, Wang H (2018) Extreme deformation characteristics and countermeasures for a tunnel in difficult grounds in southern Shaanxi, China. Environ Earth Sci 77(19):706

Li SC, Wu J, Xu ZH, Zhou L, Zhang B (2019) A possible prediction method to determine the top concealed karst cave based on displacement monitoring during tunnel construction. Bull Eng Geol Environ 78(1):341–355

Loganathan N, Poulos HG (1998) Analytical prediction for tunneling induced ground movements in clays. ASCE J Geotech Geoenviron 124(9):846–856

Lu DC, Kong FC, Du X, Shen CP, Gong QM, Li PF (2019) A unified displacement function to analytically predict ground deformation of shallow tunnel. Tunn Undergr Space Technol 88(3):129–143

Mair RJ, Taylor RN, Bracegirdle A (1993) Subsurface settlement profiles above tunnels in clays. Géotechnique 43(2):315–320

Mouratidis A (2008) The "cut-and-cover" and "cover-and-cut" techniques in highway engineering. Electron J Struct Eng 13:1–15

Muraro S, Madaschi A, Gajo A (2015) Passive soil pressure on sloping ground and design of retaining structures for slope stabilisation. Géotechnique 65(6):507–516

Ng CWW, Lee KM, Tang DKW (2004) Three-dimensional numerical investigations of new Austrian tunnelling method (NATM) twin tunnel interactions. Can Geotech J 41(3):523–539

Noferini L, Pieraccini M, Mecatti D, Macaluso G, Atzeni C, Mantovani M, Marcato G, Pasuto A, Silvano S, Tagliavini F (2007) Using GB-SAR technique to monitor slow moving landslide. Eng Geol 95(3–4):88–98

O'Rourke T, Lane P (1989) Liquefaction hazards and their effects on buried pipe-lines. Tec Rep Nat Cen Const Edu Res NCEER–89–0007. University of Buffalo, USA

Park KH (2004) Elastic solution for tunneling-induced ground movements in clays. ASCE Int J Geomech 4(4):310–318

Park KH (2005) Analytical solution for tunnelling-induced ground movement in clays. Tunn Undergr Space Technol 20(3):249–261

Peck RB (1969) Deep excavations and tunneling in soft ground. P 7th Int Conf. Soil Mech Found Eng. Mexico, 225–290

Picarelli L, Petrazzuoli S, Warren C (2002) Interazione tra gallerie e versanti, Le opere in sotterraneo in rapporto con l'ambiente. IX Cycle Conf. Rock Mech Eng, Torino, Italy, pp 219–248

Poisel R, Mair am Tinkhof K, Preh A (2016) Landslide caused damages in a gallery. Rock Mech Rock Eng 49(6):2301–2315

Puzrin AM, Schmid A (2012) Evolution of stabilised creeping landslides. Géotechnique 62(6):491–501

Sagaseta C (1987) Analysis of undrained soil deformation due to ground loss. Géotechnique 37(3):301–320

Shahin HM, Nakai T, Ishii K, Iwata T, Shou K (2016) Investigation of influence of tunneling on existing building and tunnel: model tests and numerical simulations. Acta Geotech 11(3):679–692

Song ZF, Xu XM (2012) Brief introduction of residual thrust method and its improvement. Appl Mech Mater 166:3358–3363

Song F, Wang HN, Jiang MJ (2018) Analytical solutions for lined circular tunnels in viscoelastic rock considering various interface conditions. Appl Math Model 55(3):109–130

Strack OE, Verruijt A (2002) A complex variable solution for a deforming buoyant tunnel in a heavy elastic half-plane. Int J Numer Anal Met 26(12):1235–1252

Urciuoli G, Picarelli L (2008) Interaction between landslides and man-made works. P 10th Int Symp Landslides Eng Slopes, Xi'an, China, CRC Press, 1301–1307

Vassallo R, Mishra M, Santarsiero G, Masi A (2016) Interaction of a railway tunnel with a deep slow landslide in clay shales. Procedia Earth Planet Sc 16:15–24

Verruijt A (1997) A complex variable solution for a deforming circular tunnel in an elastic half-plane. Int J Numer Anal Met 21(2):77–89

Verruijt A (1998) Deformations of an elastic half plane with a circular cavity. Int J Solids Struct 35(21):2795–2804

Verruijt A, Booker JR (1996) Surface settlements due to deformation of a tunnel in an elastic half plane. Géotechnique 46(4):753–756

Vesic AS (1961) Bending of beams resting on isotropic elastic solid. J Soil Mech Found 87(2):35–53

Vorster TE, Klar A, Soga K, Mair RJ (2005) Estimating the effects of tunneling on existing pipelines. J Geotech Geoenviron 131(11): 1399–1410

Wang TT (2010) Characterizing crack patterns on tunnel linings associated with shear deformation induced by instability of neighboring slopes. Eng Geol 115(1–2):80–95

Wang MB, Li SC (2009) A complex variable solution for stress and displacement field around a lined circular tunnel at great depth. Int J Numer Anal Met 33(7):939–951

Wang WL, Wang TT, Su JJ, Lin CH, Seng CR, Huang TH (2001) Assessment of damage in mountain tunnels due to the Taiwan Chi-Chi earthquake. Tunn Undergr Space Technol 16(3):133–150

Wang LZ, Li LL, Lv XJ (2009) Complex variable solutions for tunneling-induced ground movement. Int J Numer Anal Met 9(2):63–72

Wang TZ, Wang CM, Huang XH, Zhu HB (2016) Spatial distribution of accumulation landslide thrust based on transfer coefficient method. Int J Heat Technol 34(2):287–292

Wu J, Li SC, Xu ZH (2019) Numerical analysis of gas-liquid two-phase flow after water inrush from the working face during tunnel excavation in a karst region. Bull Eng Geol Environ 78(4):2973–3010

Yang XL, Wang JM (2011) Ground movement prediction for tunnels using simplified procedure. Tunn Undergr Space Technol 26(3): 462–471

Yang JS, Liu BC, Wang MC (2004) Modeling of tunneling-induced ground surface movements using stochastic medium theory. Tunn Undergr Space Technol 19(2):113–123

Yoo C, Kim SB (2008) Three-dimensional numerical investigation of multifaced tunneling in water-bearing soft ground. Can Geotech J 45(10):1467–1486

Yoshikoshi W, Watanabe O, Takagi N (1978) Prediction of ground settlements associated with shield tunnelling. Soils Found 18(4):47–59

Zhang ZG, Zhao QH, Xu C, Xu XY (2017) Interaction analyses between tunnel and landslide in mountain area. J Mt Sci 14(6):1124–1139

Zhang ZG, Huang MS, Xi XG, Yang X (2018) Complex variable solutions for soil and liner deformation due to tunneling in clays. ASCE Int J Geomech 18(7):04018074